

Complex energy bands in α -brass

A. Bansil and H. Ehrenreich*

Division of Engineering and Applied Physics, Harvard University, Cambridge, Massachusetts 02138

L. Schwartz†

Department of Physics, Brandeis University, Waltham, Massachusetts 02154

R. E. Watson‡

Brookhaven National Laboratory, Upton, New York 11973

(Received 26 July 1973)

The average- t -matrix approximation (ATA) is used to evaluate complex energy bands in the disordered alloy α -CuZn over a range of Zn concentrations between 0 and 30 at.%. The calculations are based on the Korringa-Kohn-Rostoker equations of band theory and on the use of atomic phase shifts obtained from renormalized-atom muffin-tin potentials. We examine the effects of charge transfer between the atomic constituents on the basis of two empirical models. Both models involve a single free parameter whose value is adjusted to guarantee agreement with the experimental shift in the optical-absorption edge as a function of Zn concentration. The effects of lattice expansion in α -brass are also included and are shown to have a significant effect on the energies of various states in the vicinity of the Fermi level. The present calculations are compared with the available experimental results on α -brass. Good agreement is found with experiments sensitive to the real parts of the energy bands, for example, the concentration dependence of both the splitting of the 5-eV peak in the optical-absorption spectrum and the neck radii as determined by some of the positron-annihilation investigations. The theory agrees only qualitatively with the results of measurements sensitive to the imaginary parts of the bands such as Dingle temperatures and residual resistivities.

I. INTRODUCTION

The understanding of the electronic structure of the disordered alloys is still not as advanced as that of the ordered crystals. Theoretical studies have been largely confined to model Hamiltonians¹⁻⁶ which do not yield details, such as the Fermi-surface topology of the alloy, which are now being measured. This provides motivation for using realistic Hamiltonians for studying the electronic properties of disordered alloys.

One theoretical approach to the problem has involved multiple-scattering theory,⁷ and in many cases the so-called coherent-potential approximation (CPA).¹ While the CPA is easy to implement for some model Hamiltonians, calculations involving a realistic Hamiltonian are considerably more complicated.⁸ The disorder, however, can often be adequately treated by simpler and even more approximate methods, such as the average- t -matrix approximation (ATA),⁹⁻¹³ which have the advantage of being simpler to implement. This paper will consider realistic alloy potentials and the predicted electronic-level structure on the basis of this approximation. Both the CPA and ATA are single-site approximations. The former, however, is self-consistent and the latter not.¹³ The self-consistent treatment of the disorder alone is not sufficient, since the atomic potentials in themselves should be treated on the same footing. Because the numerical techniques relevant to Kor-

ringa-Kohn-Rostoker (KKR)¹⁴ calculations in crystals can be taken over directly in ATA calculations for alloys, a more detailed application of this approximation seems warranted.

The case to be considered in this paper is the electronic structure of the disordered alloy α -CuZn and its experimental consequences. The potentials are described within the muffin-tin approximation. Soven¹¹ has previously considered this problem using a similar scheme with the following simplifying assumptions: (i) For calculating the properties of the conduction-band states, the d admixture is neglected, and pseudopotential amplitudes instead of t matrices are averaged; (ii) for calculating the properties of the Cu-like d states, the energy dependence of the Green's-function matrix elements ($G_{\mathbf{k}}$ in Soven's notation) is neglected. Furthermore, the calculations are made only for a limited number of states having pure- d symmetry. None of these simplifications are made in this paper.

The present approach to the problem differs from Soven's in one respect: Soven calculates spectral density functions $\rho(\vec{\mathbf{k}}, E)$ for a given $\vec{\mathbf{k}}$ and E . We regard it easier and possibly more useful for some purposes to present the electronic levels in the alloy as complex energy bands. As already noted, the calculation of the complex bands within the ATA is very similar to that of crystalline bands using a KKR approach. The evaluation of $\rho(\vec{\mathbf{k}}, E)$, however, not only involves the so-called KKR

structure functions, but also their derivatives.^{8,11} By carrying over such concepts as the Fermi surfaces from the ordered crystals to the disordered alloys, complex bands provide a more natural means of comparing the theory with many sorts of experiments, than do the spectral-density functions.

The band structure of α -brass was also calculated by Amar *et al.*¹⁵ and Pant and Joshi,¹⁶ on the basis of the virtual-crystal approximation (VCA).¹⁷ In contrast with the CPA and ATA, this approximation yields only one set of d bands rather than the two, characteristic, respectively, of Cu and Zn, and gives no information about the damping of the electronic states.

The present calculation includes the effects of the charge transfer between the constituents of the alloy. These have not been considered explicitly before even though they are known to affect the physical properties of many noble- and transition-metal alloys^{8,18-21} significantly. The previously neglected^{11,15,16} effects of the concentration dependence of the lattice constant of α -brass²² are also included here.

A brief outline of the paper and some of its principal results follows. In Sec. II, the secular equation for the disordered alloy is derived, using multiple-scattering theory.^{7,10} This secular equation is found to be a simple generalization of the usual KKR equation for the crystalline bands. The basic assumptions used in deriving this equation involve the use of the ATA within the muffin-tin spheres and the VCA outside. The renormalized-atom approach²³ is used for constructing the atomic potentials of Cu and Zn. Charge-transfer effects are described by two different models: the first is based on charged-renormalized-atom potentials; the second involves an empirical shift of the alloy muffin-tin constant. The magnitude of the transferred charge is chosen to fit the experimental change in the optical edge of α -brass as a function of Zn concentration. Some of the details relevant to Sec. II are given in the appendices. The relationship of the present approach to previous calculations based on model Hamiltonians is discussed in Appendix A. The details of the Cu and the Zn potentials used are given in Appendices B and C. The numerical methods used for solving for the complex energy bands and the Fermi-surface properties of the alloy are discussed in Appendix D.

Section III presents and discusses the calculated complex energy bands of α -brass. The shifts of the real parts of various energy levels in going from the pure crystals to the alloy with and without charge transfer between the constituents are analyzed. The Cu d bands are found to change significantly on alloying. This suggests that the VCA

calculations,^{15,16} which hold them fixed artificially, have a serious limitation. (A literal application of the VCA would cause a rapid downward shift of a *single* d band in going from Cu to Zn.)

The results for the imaginary parts of the complex bands obtained from the ATA differ by about 30% at the Fermi surface from perturbation-theory estimates. The Cu- d -band damping within the ATA is either comparable in magnitude or larger depending on how charge transfer is introduced. The Zn- d -band damping vanishes in the ATA because these d states lie below the s -muffin-tin zero of the alloy. A useful decomposition of the damping of any state in the alloy, into its angular-momentum components is described, and it is used for discussing the anisotropy of the Fermi-surface damping.

Section IV compares theory with experiment in regard to both the real energy shifts and the damping of the states. Even though the concentration dependence of the optical-absorption edge^{24,25} is adjusted to determine charge transfer, the changes in the 5-eV peak in the optical spectrum of Cu on alloying provide an independent test of the calculation. The Fermi-surface properties of α -brass are obtained in detail and are compared with positron-annihilation measurements²⁶ for the radius of the neck orbit of α -brass, and low-concentration de Haas-van Alphen measurements.²⁷ The low-temperature specific-heat coefficient^{28,29} of α -brass is also discussed.

The experimental information on the damping of the electronic states in α -brass is rather limited and the theoretical situation appears to be less satisfactory. The agreement between the experimental²⁷ and calculated Dingle temperatures is within a factor of 2. Except at small Zn concentrations, residual-resistivity measurements^{30,31} can only be interpreted qualitatively without the results of an alloy transport calculation. A low-concentration estimate leads to a qualitative agreement with experiment. In contrast with the real energy shifts, damping effects appear to be far more sensitive to the model for charge transfer. This may be an indication that these results are unreliable within the present scheme of calculations.

II. FORMULATION OF THE PROBLEM

A. Multiple-scattering theory

We assume at the outset that the alloy is described by a muffin-tin model. The disordered potential may then be written as a sum of nonoverlapping, spherically symmetric, atomic potentials, each of which is centered at a given lattice site R_n . The single-particle Hamiltonian is

$$H = p^2/2m + \sum_n v_n^{A(B)}(\vec{r}). \quad (2.1)$$

Within the muffin-tin spheres (i. e., $|\vec{r} - \vec{R}_n| < R_m$) the value of

$$v_n^{A(B)}(\vec{r}) \equiv v^{A(B)}(|\vec{r} - \vec{R}_n|)$$

depends on whether an A or B atom occupies the site n . In the region between the spheres the potential is constant. The arrangement of the A and B atoms throughout the lattice is assumed to be random.³²

The equilibrium properties of the alloy are discussed most conveniently in terms of the single-particle Green's function

$$G(E) = \langle (E - H)^{-1} \rangle.$$

For example, the spectral density $\rho(\vec{k}, E)$ and the density of states $\rho(E)$ are given by

$$\rho(\vec{k}, E) = -\pi^{-1} \text{Im} \langle \vec{k} | G(E) | \vec{k} \rangle \quad (2.2a)$$

and

$$\rho(E) = \sum_{\vec{k}} \rho(\vec{k}, E). \quad (2.2b)$$

Here the energy E is assumed to have an infinitesimal positive imaginary part and the angular brackets denote an ensemble average over all possible arrangements of the atomic constituents. If, as in Eq. (2.1), the random potential can be written as a sum of contributions from each site, it is useful to introduce the average total scattering operator $T(E)$. The relation between G and T is simply

$$G = G_0 + G_0 T G_0, \quad (2.3)$$

where $G_0 = (E - p^2/2m)^{-1}$ is the free-particle propagator. The usual equations of multiple-scattering theory^{7,10} may then be used to express T in terms of t_n , the atomic scattering matrix for the site n ,

$$t_n^{A(B)} = v_n^{A(B)} (1 - G_0 v_n^{A(B)})^{-1}. \quad (2.4)$$

The result is

$$T(\vec{k}, E) = (4\pi)^2 N \sum_{L, L'} Y_L(\vec{k}) \{ \langle t_i(k, k) \rangle \delta_{L, L'} + \langle \langle t(k, \kappa) \rangle B(\vec{k}, \kappa) [1 - \langle t(\kappa, \kappa) \rangle B(\vec{k}, \kappa)]^{-1} \langle t(\kappa, k) \rangle \rangle_{LL'} \} Y_{L'}(\vec{k}), \quad (2.10)$$

where N is the total number of atoms and the matrix elements $B_{LL'}(\vec{k}, \kappa)$ are the conventional KKR structure functions¹⁴

$$B_{LL'}(\vec{k}, \kappa) = (i)^{l+l'-1} [j_l(\kappa r) j_{l'}(\kappa r')]^{-1} \sum_{\vec{R}_n \neq 0} \int e^{i\vec{k} \cdot \vec{R}_n} G_0(\vec{r} - \vec{r}' - \vec{R}_n) Y_L(\vec{r}) Y_{L'}(\vec{r}') d\Omega_r d\Omega_{r'}. \quad (2.11)$$

Here $j_l(\kappa r)$ is a spherical Bessel function and the value of $B_{LL'}(\vec{k}, \kappa)$ is in fact independent of \vec{r} and \vec{r}' as long as both $r, r' < R_m$.³³

It should be emphasized that all available in-

$$T = \sum_n \langle t_n \rangle + \sum_{\substack{n \\ m \neq n}} \langle t_n G_0 t_m \rangle + \sum_{\substack{n \\ m \neq n \\ p \neq m}} \langle t_n G_0 t_m G_0 t_p \rangle + \dots \quad (2.5)$$

Equations (2.2)–(2.5) are exact and, in principle, provide a complete description of the average alloy. Neglecting all contributions to (2.5) due to fluctuations in the effective scattering, we obtain the present version of the average- t -matrix approximation

$$T = \sum_n \langle t_n \rangle + \sum_{\substack{n \\ m \neq n}} \langle t_n \rangle G_0 \langle t_m \rangle + \sum_{\substack{n \\ m \neq n \\ p \neq m}} \langle t_n \rangle G_0 \langle t_m \rangle G_0 \langle t_p \rangle + \dots, \quad (2.6)$$

where

$$\langle t_n \rangle = x t_n^A + (1-x) t_n^B, \quad (2.7)$$

and x is the relative concentration of A atoms.

For the purpose of evaluating the (complex) quasiparticle energy bands, it is most convenient to work with the momentum representation of Eq. (2.6), i. e., with the quantity $T(\vec{k}, E) \equiv \langle \vec{k} | T(E) | \vec{k} \rangle$. As various authors have shown,^{8,10-12} $T(\vec{k}, E)$ can be expressed directly in terms of the matrix elements $t(\vec{k}, \vec{k}')$ of the atomic scattering operators (2.4). Since the atomic potentials are spherically symmetric, $t(\vec{k}, \vec{k}')$ is diagonal in its angular-momentum indices and can be written in terms of the real spherical harmonics $Y_{lm}(\vec{k}) \equiv Y_L(\vec{k})$ as

$$t(\vec{k}, \vec{k}') = (4\pi)^2 \sum_L Y_L(\vec{k}) t_l(k, k') Y_L(\vec{k}'). \quad (2.8)$$

In the special case, $k = k' = E^{1/2} \equiv \kappa$, the quantities $t_l(k, k')$ are related to the familiar scattering phase shifts $\eta_l(\kappa)$:

$$t_l(\kappa, \kappa) = -\kappa^{-1} e^{i\eta_l(\kappa)} \sin[\eta_l(\kappa)]. \quad (2.9)$$

Substituting Eqs. (2.8) and (2.9) into (2.7) and then into (2.6), the series can be summed exactly, and the resulting expression for $T(\vec{k}, E)$ is:

formation concerning the electronic spectrum is contained in $T(\vec{k}, E)$, and, in particular, that the energy eigenvalues are specified by the singularities of $T(\vec{k}, E)$. For example, in a perfect crystal,

given a vector \vec{k} in the first Brillouin zone, these singularities occur at a sequence of real energies $E^{(n)}(\vec{k})$ and determine the energy bands of the solid. By contrast, in the disordered alloy the singularities are found at complex energies $E^{(n)}(\vec{k}) = E_1^{(n)}(\vec{k}) + iE_2^{(n)}(\vec{k})$ and are associated with long lived quasi-particle states³⁴ only if $E_2(\vec{k})/E_1(\vec{k}) \ll 1$. Inspection of Eq. (2.10) reveals that, just as in the perfect crystal, the singularities of $T(\vec{k}, E)$ are determined by the vanishing of the determinant associated with the inverse matrix in the second term, i. e., by the equation

$$|\delta_{LL'} - \langle t_l(\kappa, \kappa) \rangle B_{LL'}(\vec{k}, \kappa)| = 0. \quad (2.12)$$

This is the alloy-KKR (AKKR) equation upon which the calculations of this paper are based.^{35,36} In a perfect crystal Eq. (2.12) reduces to the KKR equation of band theory. Equation (2.12) requires two basic units of input: First, the matrix $B_{LL'}(\vec{k}, \kappa)$ which is determined by the structure of the periodic lattice and second, the constituent potentials $v^{A(B)}$ which determine both the average scattering matrix elements $\langle t_l(\kappa, \kappa) \rangle$ [through Eq. (2.7)] and also, the uniform muffin-tin potential \bar{V}_0 in the region between the spheres.

In the present calculations the point lattice of the alloy is assumed to be periodic. The Wigner-Seitz radii of Cu and Zn must therefore be taken as identical. The structure functions $B_{LL'}(\vec{k}, \kappa)$ are then evaluated exactly as they would be in a perfect-crystal band-structure calculation.³³ Similarly, if the effects of charge transfer can be neglected, then the atomic potentials $v^{A(B)}$ can be evaluated by methods identical to those used in the pure crystals. However, the corresponding muffin-tin constants V_0^A and V_0^B will not in general be equal, so that a further approximation is required to specify the alloy-muffin-tin potential. In many systems of interest V_0^A and V_0^B are nearly equal and the use of an average muffin tin

$$\bar{V}_0 = xV_0^A + (1-x)V_0^B \quad (2.13)$$

is then reasonable. On the other hand, if charge transfer or atomic size effects cannot be neglected, then the proper choice of the atomic potentials is a considerably more delicate matter in the alloy than it is in the pure crystal. This point is discussed in Sec. IIB where it is argued that the incorporation of charge transfer requires either an adjustment of the value of the atomic potentials within the muffin-tin spheres, or, an empirical shift of the uniform potential \bar{V}_0 away from its virtual crystal value (2.13). A proper account of atomic size effects would involve considering a nonperiodic point lattice and is therefore beyond the scope of the present theoretical framework.

On the basis of a study of several tight-binding-

model Hamiltonians, Schwartz *et al.*¹³ have examined the validity of the average- t -matrix equations in disordered alloys. These authors have shown that in many cases the ATA provides an excellent first approximation to the self-consistent CPA. Although the results of both the present paper and Ref. 13 are based on the approximate Eq. (2.6), there is nevertheless an important difference between them. When dealing with model Hamiltonians, the simplest procedure is to assume that the Green's function $G_0(E)$ appearing in (2.6) corresponds to the perfect-host lattice. It is then possible to show that the ATA is exact to first order in the impurity concentration x . Similarly if $G_0(E)$ corresponds to the virtual crystal [i. e., $G_0(E) = (E - \langle H \rangle)^{-1}$] then the average- t -matrix equations are symmetric with respect to the interchange of A and B atoms and are correct to lowest order in x and $1-x$ in the appropriate limits. Having made these statements, it should be emphasized that the calculations discussed in Ref. 13 are tractable only because the various Green's functions are easily evaluated within the framework of the tight-binding models. However, this is not the case for the more realistic Hamiltonians under consideration in the present paper. Indeed, for the muffin-tin model, even a calculation of the perfect-host Green's function would involve a numerically complicated integration over the Brillouin zone. While it is certainly possible to formulate the AKKR equations corresponding to an arbitrary reference Green's function (see Appendix A), their solution is relatively straightforward only if, as in Eq. (2.12), $G_0(E)$ corresponds to the empty-lattice Hamiltonian: $H_0 = p^2/2m$. Given this choice, however, it is no longer true that the ATA is correct to first order in the impurity concentration x . Nevertheless, despite this apparent difficulty, the results for the CuZn alloy presented in Secs. III and IV appear to be quite reasonable, and suggest that this approximation is not serious for practical calculations of many of the physical properties of the alloy.

B. Renormalized-atom potentials and charge transfer

The renormalized-atom approach²³ has been used to construct l -dependent Cu and Zn potentials. For each constituent, renormalized wave functions $\psi_i(\vec{r})$, corresponding to the free-atom orbitals $\phi_i(\vec{r})$, are defined by truncating $\phi_i(\vec{r})$ at the Wigner-Seitz radius R_{ws} and then multiplying by a constant N to insure normalization within the Wigner-Seitz sphere. Thus

$$\psi_i^{A(B)}(\vec{r}) = \begin{cases} N^{A(B)} \phi_i^{A(B)}(\vec{r}), & r < R_{ws} \\ 0, & r > R_{ws} \end{cases} \quad (2.14a)$$

and $N^{A(B)}$ are constants such that

$$\int_{r < R_{ws}} |\psi_i^{A(B)}(\vec{r})|^2 d^3r = 1. \quad (2.14b)$$

Self-consistent Hartree-Fock wave functions $\phi_i(\vec{r})$ are used to determine the $\psi_i(\vec{r})$ from which the single-site renormalized-atom potentials are then calculated. These potentials contain a full Coulomb correlation hole and include exchange effects within the atomic Hartree-Fock approximation. Further details are given in Appendix B.

While each Wigner-Seitz cell in a monatomic pure crystal is neutral, this will in general not be the case in either ordered or disordered binary alloys.^{6,18-21} For example, the explanation of the optical properties of Ag-Au⁶ and other Au-based²⁰ alloys requires that charge be transferred between the constituents. Since our potentials are not determined self-consistently (in terms of the calculated electronic charge distribution), the incorporation of charge transfer requires an *ad hoc* adjustment of one or another feature of the neutral atomic potentials described above. Two different models to include such effects have been explored. Each involves an empirical parameter, whose value is adjusted to obtain agreement between the calculated and experimental values of the shift in the fundamental optical edge as a function of Zn concentration.

The first method, the charge-renormalized (CR) model, is physically the most natural extension of the neutral-renormalized-atom concept. For a given constituent, the potential is modified by choosing the renormalization constant in Eq. (2.14a) such that

$$(N_c^{A(B)})^2 = (N_n^{A(B)})^2 (1 + \Delta^{A(B)}).$$

Here the subscripts c and n refer to the charged and neutral renormalized atoms, respectively. This procedure leads to a net charge $e\Delta^{A(B)}$ within the $A(B)$ Wigner-Seitz cell. To insure that the total alloy is electrically neutral, the values of $\Delta^{A(B)}$ must satisfy

$$x\Delta^A + (1-x)\Delta^B = 0. \quad (2.15)$$

Typical values of Δ are, for example, $\Delta^{\text{Cu}(\text{Zn})} = 0.057$ (-0.134) at an impurity concentration of 30%. These values are comparable to the estimates of 0.075 in β -brass (ordered phase of composition $\text{Cu}_{0.5}\text{Zn}_{0.5}$) of Mott and Arlinghaus.²¹ Interestingly, the former estimate was obtained from stability considerations pertaining to the ordered phase.

Inside the Cu and Zn atomic spheres the change in potential brought about by the CR adjustment is found to vary slowly as a function of r . This fact suggests that the essential features of the CR model could be reproduced by a simpler approach in which the potential within the Cu (Zn) muffin-tin sphere was simply shifted by a constant $\delta V^{\text{Cu}(\text{Zn})}$. Indeed, the results obtained with this empirical shift (cf. Appendix C) are in remarkable agreement with those of the CR model. Physically, the transferred charge associated with the constant shift of the potentials is confined to a spherical shell at the muffin tin radius, its value being simply $e\Delta^{\text{Cu}(\text{Zn})} = \delta V^{\text{Cu}(\text{Zn})}R_m$. In view of Eq. (2.15) it is then clear that within this simplified framework the average change in the potentials within the muffin-tin spheres vanishes, i. e.,

$$x\delta V^{\text{Cu}} + (1-x)\delta V^{\text{Zn}} = 0. \quad (2.16)$$

Since the results of the CR model are essentially

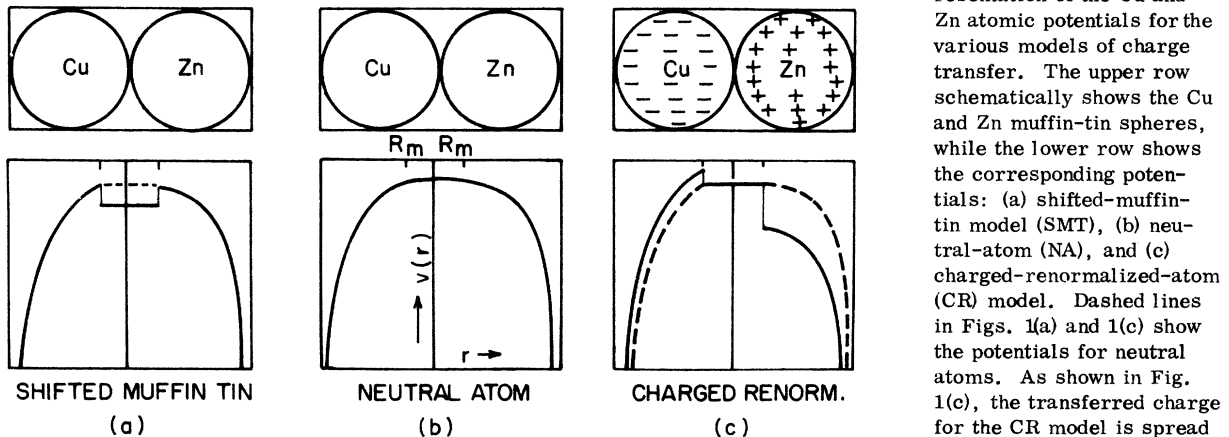


FIG. 1. Schematic representation of the Cu and Zn atomic potentials for the various models of charge transfer. The upper row schematically shows the Cu and Zn muffin-tin spheres, while the lower row shows the corresponding potentials: (a) shifted-muffin-tin model (SMT), (b) neutral-atom (NA), and (c) charged-renormalized-atom (CR) model. Dashed lines in Figs. 1(a) and 1(c) show the potentials for neutral atoms. As shown in Fig. 1(c), the transferred charge for the CR model is spread over the whole of the muffin-tin sphere.

TABLE I. Complex energies, $(E_1, E_2) \equiv E_1 + iE_2$ in rydbergs, at symmetry points in α -Cu_xZn_{1-x} having Cu lattice constants for different charge-transfer models.

State	Cu _{0.85} Zn _{0.15}			Cu _{0.7} Zn _{0.3}		
	Cu	Charged renormalized (CR)	Shifted muffin tin (SMT)	Charged renormalized (CR)	Shifted muffin tin (SMT)	Neutral atom (NA)
Γ_1	0.0161	(-0.0068, 0.0)	(-0.0396, -0.0007)	(-0.0297, 0.0)	(-0.095, -0.0010)	(-0.009, 0.0)
$\Gamma_{25'}$	0.3808	(0.4108, -0.0029)	(0.3776, -0.0046)	(0.4398, -0.0061)	(0.3743, -0.0125)	(0.3824, -0.0047)
Γ_{12}	0.4510	(0.4705, -0.0036)	(0.4394, -0.0048)	(0.4894, -0.0075)	(0.4269, -0.0133)	(0.4314, -0.0056)
X_1	0.2178	(0.2656, -0.0021)	(0.2259, -0.0029)	(0.3141, -0.0044)	(0.2348, -0.0102)	(0.2691, -0.0027)
X_3	0.2580	(0.3061, -0.0016)	(0.2708, -0.0035)	(0.3535, -0.0041)	(0.2825, -0.0117)	(0.3001, -0.0033)
X_2	0.4997	(0.5119, -0.0041)	(0.4820, -0.0052)	(0.5238, -0.0085)	(0.4660, -0.0135)	(0.4665, -0.0061)
X_5	0.5165	(0.5264, -0.0043)	(0.4969, -0.0054)	(0.5357, -0.0086)	(0.4764, -0.0137)	(0.4788, -0.0063)
$X_{2'}$	0.8372	(0.8124, -0.0111)	(0.7748, -0.0015)	(0.7894, -0.0163)	(0.7128, -0.0023)	(0.8002, -0.0029)
L_1^{\dagger}	0.2347	(0.2741, -0.0042)	(0.2398, -0.0029)	(0.3150, -0.0074)	(0.2461, -0.0098)	(0.2743, -0.0029)
L_3^{\dagger}	0.3739	(0.4059, -0.0027)	(0.3719, -0.0042)	(0.4359, -0.0060)	(0.3683, -0.0126)	(0.3783, -0.0046)
L_5^{\dagger}	0.5028	(0.5144, -0.0041)	(0.4847, -0.0051)	(0.5259, -0.0084)	(0.4659, -0.0136)	(0.4688, -0.0062)
$L_{2'}$	0.6193	(0.5961, -0.0080)	(0.5495, -0.0010)	(0.5758, -0.0112)	(0.4795, -0.0014)	(0.5874, -0.0018)
L_1^{\dagger}	1.0018	(0.9728, -0.0122)	(0.9474, -0.0044)	(0.9420, -0.0208)	(0.8923, -0.0083)	(0.9323, -0.0068)
E_d^{Cu}	0.4088	0.4347	0.4023	0.4596	0.3953	0.4020
E_d^{Zn}		-0.254	-0.088	-0.224	-0.091	-0.084
E_F	0.687	(0.710, -0.0091)	(0.677, -0.0031)	(0.731, -0.0147)	(0.662, -0.0068)	(0.723, -0.0042)

identical to those obtained with the uniform shifts δV , an equation of the form (2.16) can be expected to hold approximately for the charged renormalized atomic potentials. This point is of some importance since in using the CR model we are assuming that the individual atomic potentials are not modified any further when the charged atoms are put together to form the alloy. Any effects of a Madelung potential,³⁷ which [in view of Eq. (2.16)] may well be weak in a random alloy, are thereby neglected.

The second approach to charge transfer, the shifted-muffin-tin (SMT) model, involves lowering the *sp*-muffin-tin constant of the alloy (cf. Fig. 1).

This adjustment has the effect of shifting all the levels of the alloy downwards, and of lowering the conduction band with respect to the *d* bands. The shift in energy of a given state is proportional to the fraction of its charge density residing in the muffin-tin region. Accordingly, within the *d* bands, the bonding states (e.g., X_3) are lowered more than the antibonding states (e.g., X_5), and the adjustment may be thought to correspond to an increase in the bonding charge, i.e., to an increase in the covalent character of the chemical bond. In the SMT model the charge-transfer parameter Δ^{Cu} is determined by the shift of E_d^{Cu} with respect to a typical conduction-band state say Γ_1 , induced

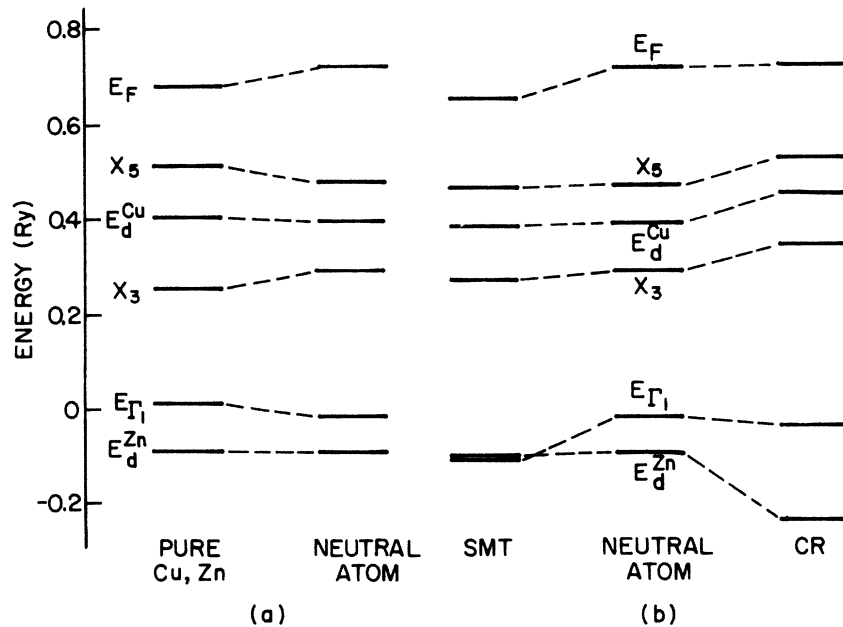


FIG. 2. Energy-level diagram for pure crystals and α -Cu_{0.7}Zn_{0.3}: (a) pure crystals and the NA alloy, (b) the NA, the SMT, and the CR models. The energy zero is taken to be -0.8341 Ry, which is the muffin-tin zero for pure Cu.

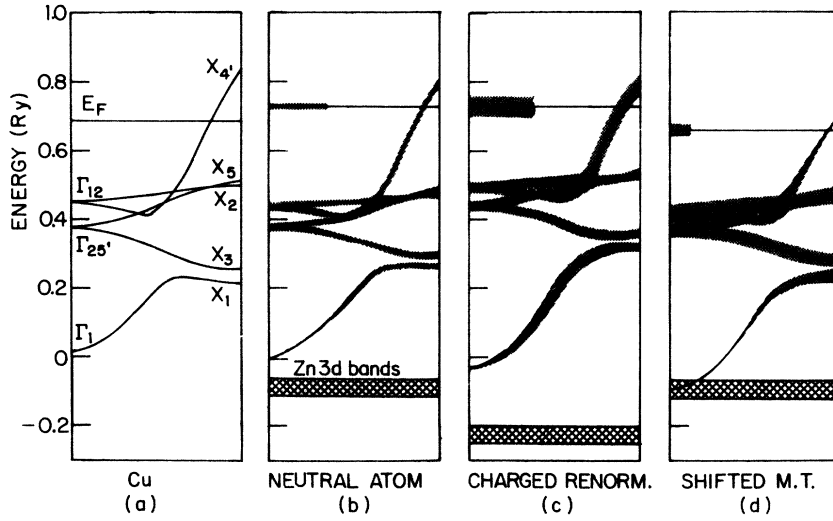


FIG. 3. Calculated energy bands for pure Cu and α -Cu_{0.7}Zn_{0.3} from $\Gamma \rightarrow X$: (a) pure Cu, (b)–(d) α -Cu_{0.7}Zn_{0.3} for different charge-transfer models. The shading of the bands corresponds to four times the imaginary part of the complex energies. The shading around the Fermi energy corresponds to four times the average damping on the Fermi surface. The Zn 3d bands are shown as a hatched band. The energy zero is taken to be -0.8341 Ry.

by the muffin-tin adjustment

$$\delta(E_d^{\text{Cu}} - E_{\Gamma_1}) = \Delta^{\text{Cu}} F_0, \quad (2.17)$$

where F_0 is a Coulomb integral whose value is typically 1 Ry.²³ We emphasize that Eq. (2.17) is intended to provide only a crude estimate of the value of Δ^{Cu} to be associated with the empirical shift in \bar{V}_0 . At a Zn concentration of 0.3, the SMT value of Δ^{Cu} is found to be 0.079.

III. COMPLEX ENERGY BANDS

The results of our calculations are summarized

in Table I and Figs. 2 and 3. Table I gives the real and imaginary parts of the low-lying energy levels at the symmetry points Γ , X , and L for the 15 and 30 at. % alloys. Figure 3 shows the complex energy bands along the $[100]$ direction for pure Cu and Cu_{0.7}Zn_{0.3}. The imaginary parts of the energies are represented by the vertical lines [of length $4|E_2^{(g)}(\vec{k})|$] through each band. Results both for the neutral atom (NA) as well as the CR and SMT models are presented. A typical plot of the complex energy bands along the principal symmetry directions of the crystal is shown in Fig. 4.

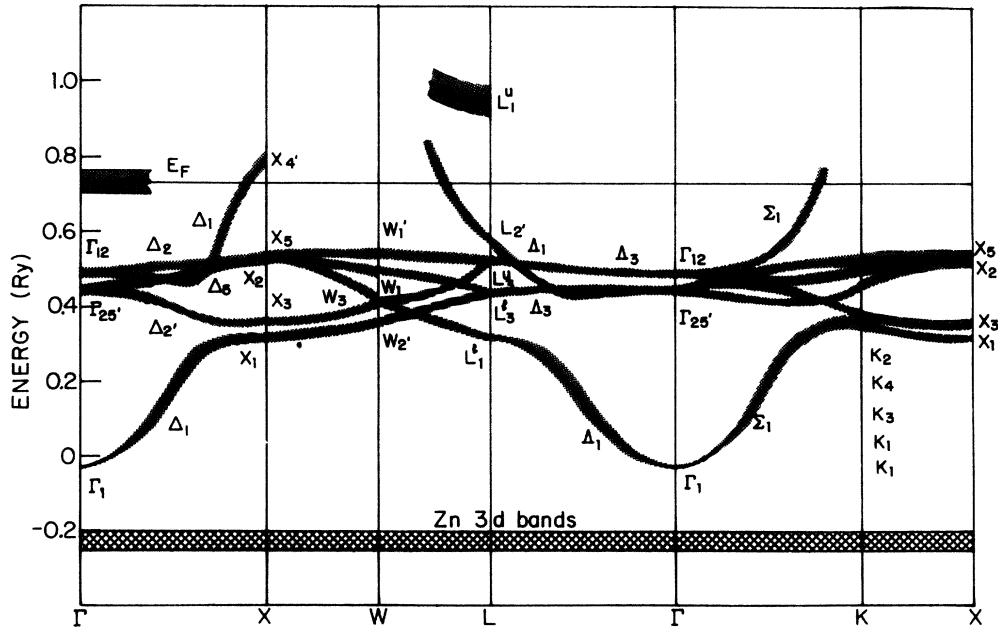


FIG. 4. Calculated energy bands for α -Cu_{0.7}Zn_{0.3} for the charged-renormalized atom model. See caption for Fig. 3 for the meaning of the shading.

A. Real parts of the complex bands

The qualitative features of our results are most easily understood in terms of the behavior of the real parts of several of the most important energy levels of the alloy. The levels we consider are: the bottom of the conduction band E_{Γ_1} , the Fermi level E_F , the centers of the Cu and Zn d bands E_d^{Cu} and E_d^{Zn} , and finally, the bonding and antibonding states X_3 and X_5 that determine the characteristic width of the Cu d bands. The energy shifts in going from pure Cu to neutral atom $\text{Cu}_{0.7}\text{Zn}_{0.3}$, and subsequently to the alloy including charge-transfer effects, are indicated in Figs. 2(a) and 2(b), respectively. The Zn d level shown on the left side of Fig. 2(a) is that corresponding to a hypothetical Zn crystal having the fcc structure of Cu and the same lattice constant.

The principal features associated with the addition of 30% Zn to pure Cu, without including charge transfer [Fig. 2(a)] are the following: the appearance of separate Zn d bands, a narrowing of the Cu d bands, a downward shift of E_{Γ_1} , and an increase in width of the occupied portion of the alloy conduction band. The present calculations yield two sets of d bands due to the fact that we have averaged t matrices rather than potentials as in the virtual-crystal approximation (VCA). In fact, a direct application of the VCA would predict a single d band whose center of gravity would shift downwards with increasing Zn concentration.³⁸ The reduction in width of the Cu d bands is associated with the fact that in a random alloy the number of Cu atoms surrounding a given Cu site (and hence the effective number of Cu-Cu transfer integrals) decreases in direct proportion to the concentration of Zn atoms. Indeed, inspection of columns one and six of Table I indicates that the variation of $\Delta E_d^{\text{Cu}} \equiv X_5 - X_3$ is essentially linear^{39,40} in the concentration $1 - x$ of Zn atoms.

In contrast to the behavior of the d bands, the changes in the NA conduction bands are easily understood in terms of a virtual-crystal model.^{41,42} For example, a linear downward shift in E_{Γ_1} is expected⁴³ since the Zn potential is more attractive than that of Cu and the $\vec{k} = 0$ state, having the most uniform wave function, tends to sample the average potential in the alloy. The rise in the Fermi level E_F is simply due to the increased average number of electrons per atom. Its magnitude, however, is less than a Cu-based rigid-band model⁴⁴⁻⁴⁶ would predict because the lowering of E_{Γ_1} acts to depress the entire conduction band. Next, we consider the width of the occupied portion of the NA conduction band ($E_F - E_{\Gamma_1}$) as a function of Zn concentration. This quantity is of interest because earlier calculations^{11,15,16} have not explicitly evaluated E_F . Instead, $E_F(x)$ was esti-

mated from the calculated value of $E_{\Gamma_1}(x)$, by requiring that the increase in the width of the occupied conduction band be the same as that obtained from a Cu-based rigid-band model. In the present calculation, E_F is evaluated by a \vec{k} -space integration. For the $\text{Cu}_{0.7}\text{Zn}_{0.3}$ NA alloy the increase in $(E_F - E_{\Gamma_1})$ is 0.061 Ry, whereas the rigid-band model gives an increase of 0.088 Ry. The difference is due to the decrease in the total number of Cu d states on alloying, and the consequent smaller expulsion of s states from the d -band region. It is interesting to note, however, that once the effects of charge transfer are added [cf. Fig. 2(b)], there is a compensating increase in $(E_F - E_{\Gamma_1})$, and the final results are in agreement with the earlier rigid-band estimates.

The further changes that occur when charge transfer is included are illustrated in Figs. 1, 2(b), 3(c), and 3(d). It was noted in Sec. IIB that in going from the NA to the CR model the average change in the alloy potential is small. Consequently the levels E_{Γ_1} and E_F are not expected to vary significantly. By contrast, the Cu d band rises because the Cu atomic potential is raised. [See Figs. 1 and 2(b).] As expected, this increases E_F slightly. Similarly, due to the lowering of the Zn atomic potential, E_d^{Zn} drops.

In connection with the SMT model, we note that as a result of the lowering of the average sp muffin tin, all levels in the alloy are depressed. The shift in energy of a given state depends on the fraction of its charge found in the muffin-tin region. Thus, the conduction-band states, whose wave functions tend to be more uniform, are affected more than a typical d level. Similarly, within the Cu d bands, the antibonding state X_5 is essentially unaffected, while the lowering of the bonding state X_3 is more apparent.

It is clear from Fig. 2(b) that, as far as the optical-absorption edge is concerned, the principal effect of the adjustments involved in either the CR or SMT models is to reduce the gap between the top of the Cu d bands and the Fermi level. In both cases therefore, the value of the charge-transfer parameter can be fixed by requiring agreement between the calculated and experimental values of the shift in the optical edge corresponding to the transition $L_3^u - E_F$.

While the two models are similar in this respect, one possibly important shortcoming may be that the charge transfer is determined by a single gap at one symmetry point of the Brillouin zone. Their predictions regarding other physical properties may well differ. For example, in connection with the cohesive energy, the downward shift of the bands introduced by the SMT model would most likely lead to results different from those of the CR model where the adjustment tends to spread

TABLE II. Shifts in energy levels in rydbergs of Cu and α -Cu_{0.7}Zn_{0.3} when the lattice constant is increased by 2%. Complex energies are denoted as in Table I.

State	Cu		α -Cu _{0.7} Zn _{0.3}	
	DFJ ^a	Renormalized atom	SMT	CR
Γ_1	0.0374	-0.0027	(-0.0013, 0.0)	(-0.0019, 0.0)
Γ_{12}	0.0092	-0.0487	(-0.0463, 0.0022)	(-0.0458, 0.0019)
$\Gamma_{25'}$	0.0148	-0.0412	(-0.0409, 0.0020)	(-0.0404, 0.0015)
X_1	0.0292	-0.0216	(-0.0260, 0.0022)	(-0.0262, 0.0008)
X_3	0.0248	-0.0278	(-0.0313, 0.0023)	(-0.0315, 0.0012)
X_2	0.0054	-0.0537	(-0.0520, 0.0021)	(-0.0497, 0.0020)
X_5	0.0040	-0.0551	(-0.0515, 0.0021)	(-0.0509, 0.0019)
$X_{4'}$	0.0060	-0.0356	(-0.0326, 0.0002)	(-0.0339, -0.0005)
L_1^I	0.0268	-0.0237	(-0.0269, 0.0020)	(-0.0268, 0.0006)
L_3^I	0.0154	-0.0401	(-0.0399, 0.0022)	(-0.0400, 0.0015)
L_3^U	0.0052	-0.0537	(-0.0504, 0.0021)	(-0.0499, 0.0019)
$L_{2'}$	0.0174	-0.0240	(-0.0210, 0.0001)	(-0.0228, -0.0002)
L_1^U	-0.0202	-0.0672	(-0.0641, 0.0008)	(-0.0635, 0.0001)
$L_1^U-L_{2'}$	-0.0376	-0.0432	(-0.0431, 0.0007)	(-0.0407, 0.0003)
$X_{4'}-X_5$	0.0020	0.0195	(0.0189, -0.0020)	(0.0170, -0.0024)
X_5-X_3	-0.0208	-0.0273	(-0.0202, -0.0002)	(-0.0194, 0.0007)

^aReference 47.

the bands apart. A detailed study of this point, of course, requires a knowledge of the complete density of electronic states and is beyond the scope of the present calculations. In addition we note that the CR and SMT models lead to qualitatively different predictions regarding the relative positions of the Cu and Zn d bands [cf. Fig. 2(b)]. In the SMT model the Zn d bands lie very close to E_{Γ_1} , whereas in the CR model they lie approximately 0.2 Ry below the bottom of the alloy conduction band. Also, the separation of the Cu and Zn d bands is approximately 0.2 Ry larger in the CR model. X-ray-photoemission experiments on α -brass, and particularly those that place the Zn d level relative to E_F , would help to resolve some of these questions.

Finally, we consider the influence of lattice expansion (here assumed to be uniform) on the band structure of α -brass. Experimentally, the lattice constant of α -Cu_{0.7}Zn_{0.3} is found to be approximately 2% larger than that of Cu.²² Within the renormalized-atom framework, the neutral-atom potentials for the expanded lattice are constructed by renormalizing the wave functions within the corresponding larger Wigner-Seitz sphere, and are used to calculate the band structures of Cu and α -CuZn on the expanded lattice. Table II lists the shifts in the energies of some of the low-lying levels at symmetry points Γ , X , and L for Cu and α -Cu_{0.7}Zn_{0.3} on expanding the lattice, along with the shifts in energy levels obtained from the calculations of Davis, Faulkner, and Joy⁴⁷ for pure Cu. The alloy results are obtained for the charged atoms within the shifted-muffin-tin and the charge-

renormalized-atom schemes.

Consider first the results for Cu as a function of lattice dilation. Comparing the first and second columns of Table II, we see that the shifts of the energy levels obtained from the present calculations and those of Ref. 47 are very different. This discrepancy is due to the differences in the construction of the crystalline potentials.⁴⁸ We remark, however, that the behavior of the various energy gaps [e.g., ($L_1^U - L_{2'}$), ($X_{4'} - X_5$), and ($X_5 - X_3$)] for the two calculations are in reasonable agreement. Furthermore, the results given in Table II show that the shifts in the energy levels obtained from the present calculations on expanding the lattice are almost the same for Cu on the one hand and α -Cu_{0.7}Zn_{0.3} (for both the charged-renormalized-atom and shifted-muffin-tin models) on the other. We shall assume that the same holds if one were to start from the results of Davis, Faulkner, and Joy for pure Cu and go to a brass alloy calculated using their scheme for constructing potentials. Therefore, for reasons pointed out in Ref. 48, the changes in the band structure of Cu with lattice constant will be used to infer the effects of lattice expansion on the energy bands of α -brass. Thus, in comparing the present results with various optical and Fermi-surface experiments, the energy bands calculated on the undiluted lattice will be corrected for lattice expansion simply by adding the shifts for pure Cu obtained from the results of Ref. 47, which are in excellent agreement with experiments concerning the pressure dependence of the energy bands of Cu.

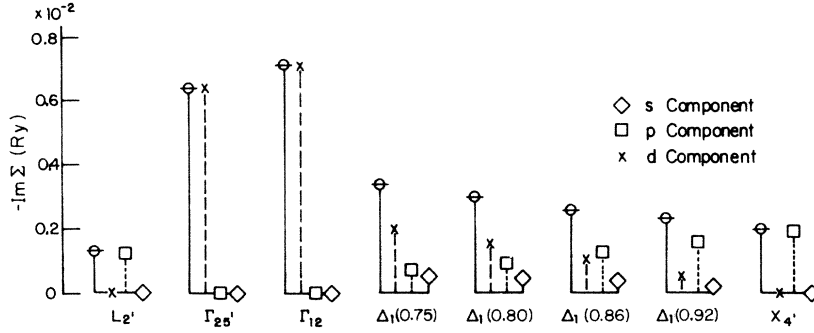


FIG. 5. Decomposition of $\text{Im}\Sigma$, a measure of the damping for electronic states in $\alpha\text{-Cu}_{0.8}\text{Zn}_{0.2}$, into l components, for the SMT model. The circles attached to the solid lines give the total damping, while the short horizontal bars give the sum of the s , p , and d components. The diamonds, the squares, and the crosses give the s , p , and d components of the damping, respectively.

B. Imaginary parts of the complex bands

The magnitude of the damping of conduction-band states obtained from the present calculations is consistent with the results of an elementary perturbation-theory estimate. The potentials seen by the conduction states in pure Cu and in a hypothetical crystal of Zn on a Cu lattice are not very different. A typical dimensionless parameter characterizing this difference is $(E_{\Gamma_1}^{\text{Cu}} - E_{\Gamma_1}^{\text{Zn}}) / (\text{occupied conduction bandwidth}) \approx (E_{\Gamma_1}^{\text{Cu}} - E_{\Gamma_1}^{\text{Zn}}) / 1 \text{ Ry} = 0.072 \ll 1$. Accordingly perturbation theory^{44,49,50} may be used to estimate the average damping on the Fermi surface of α -brass. If we define the scattering potential as $\delta V = (v^{\text{Zn}} - v^{\text{Cu}})$ and assume that the conduction band of pure Cu can be represented as a free-electron band with $k_F = 0.72 \text{ a. u.}$ then, to lowest order in x , the imaginary part of the energy of a state at the Fermi level is⁵¹

$$E_2(k_F) = x \left(\frac{2\pi\hbar^2 n}{mk_F} \right) \sum_{l=0}^{\infty} (2l+1) \sin^2(\delta_l(E_F)). \quad (3.1)$$

Here $\delta_l(E_F)$ is the l th phase shift (evaluated at the Fermi energy) corresponding to the potential δV , m is the free-electron mass, and n is the number of Cu conduction electrons per unit volume. Using the neutral-atom Cu and Zn atomic potentials to evaluate δV and then δ_l , Eq. (3.1) gives $E_2(k_F) = 3.0 \times 10^{-4} \text{ Ry}/(\text{at.}\% \text{ Zn})$. This result is to be compared with the average Fermi-surface damping calculated in the ATA: $E_2(k_F) = 2.0 \times 10^{-4} \text{ Ry}/(\text{at.}\% \text{ Zn})$.

In order to discuss the results of ATA calculations for the imaginary parts of several typical energy levels in the alloy, it is useful to introduce a decomposition of the damping of a given state into its angular-momentum components. For this purpose, the l th component of the damping is defined as the value of $E_2(\vec{k})$ obtained by solving the AKKR equation with all of the impurity phase shifts except the l th set equal to those of the host. These components are easily calculated and results for states at several of the principal symmetry points in the Brillouin zone are shown in Fig. 5. The results obtained for the SMT model

are shown, and they are typical of the NA and the CR models also. First, in all cases the damping of each state is found to be equal (within the numerical accuracy of our calculations) to the sum of s , p , and d components and second, the relative strength of each component of the damping reflects the angular-momentum character of the associated state.^{27,46,52-56} Thus in the pure d states Γ_{12} and $\Gamma_{25'}$ only the $l=2$ component of the damping is nonvanishing, while for the p states X_4' and $L_{2'}$ only the $l=1$ component contributes. Note also, that along a series of states (conduction-band states of symmetry Δ_1 are shown) changes in the weighting of the damping components track the variation in the angular-momentum components of the corresponding wave functions. For example, as the symmetry point X_4' is approached, the d and s components decrease while the p component increases.

Finally, we consider the anisotropy of the damping on the Fermi surface.⁵⁷ Results obtained from the CR and SMT models are shown in Fig. 6. It is evident from column five of Table I, that in the SMT model the damping of s or p states (e.g., Γ_1 or $L_{2'}$) is an order of magnitude smaller than that of the pure d states (e.g., Γ_{12} and $\Gamma_{25'}$). Accordingly, in this model the anisotropy of the damping is expected to reflect variations in the

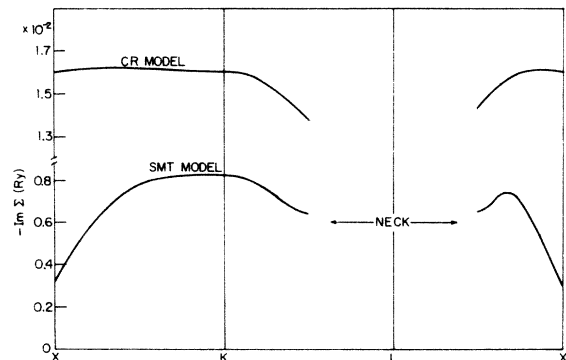


FIG. 6. Anisotropy of the damping of the Fermi surface of $\alpha\text{-Cu}_{0.7}\text{Zn}_{0.3}$ for the SMT and CR models.

d character of the states on the Fermi surface. Thus the damping along the symmetry direction K is the largest, because the d admixture is the greatest in this direction. By contrast, the anisotropy of the damping obtained from the CR model is much less marked. As we noted in Sec. II B, the SMT adjustment does not change the value of the difference potential ($v^{\text{Zn}} - v^{\text{Cu}}$), whereas in the CR model this difference is increased by a constant. This increase in the scattering potential is confined to the interior of the muffin-tin spheres, a region that is more easily accessible to wave functions of low angular momentum. The CR adjustment therefore tends to increase the damping of the s and p states, thus reducing the relative importance of the d component and the concomitant anisotropy. As noted in Sec. III A, further experimental evidence is required in order to understand what kind of charge-transfer model is the most realistic. Dingle-temperature measurements for different orbits on the Fermi surface would be useful in providing detailed maps of the Fermi-surface damping,^{58,59} thereby helping to resolve this question.

IV. COMPARISON WITH EXPERIMENT

A. Optical properties

The results of the present calculations are summarized in Figs. 7(a) and 7(b) whose discussion forms the principal topic of this subsection.

The inset in Fig. 7(a) shows the dominant features of the experimental optical-absorption spectrum and how they change with concentration.²⁵ The optical-absorption spectrum of pure Cu, given by the dashed line, shows an edge at approximately 2 eV and a large peak at 5 eV. The solid line shows that on alloying with Zn the edge moves to higher energy and the peak splits. The dominant portion (referred to as "Lower") moves to lower energy faster than the "Upper" rather more diffuse peak. Earlier results of Bionde and Rayne²⁴ agree with the observed shift. The splitting, however, was not observed in their work.

In the present comparison the shift of some of the principal optical transitions as calculated using the shifted-muffin-tin and charge-renormalized models are compared with those observed experimentally. Even though the large peak in the observed optical structure may arise from relatively large regions of the Brillouin zone,^{60,61} for the present purposes these transitions will be associated with gaps at high-symmetry points. In Cu at least, these gaps lie energetically close to the peaks.^{62,63} It is to be emphasized that we compare here the shifts of the optical structure with concentration rather than absolute magnitudes. The observed absorption edge, corresponding to the $L_3^u \rightarrow E_F$ transition is actually predicted to occur at

2.6 eV for Cu by the potential used here, which is higher than the experimental value by about 0.5 eV. This kind of discrepancy is not unusual in first-principles calculations.^{15,64} In the present calculations, the magnitude of the transferred charge was chosen to reproduce the correct concentration dependence of the principal edge for the two models discussed in Sec. II B. This is possible, since the results of Sec. III A showed that the Cu-Zn charge transfer reduces the gap between the upper d -band edge and the Fermi level. For zero charge transfer, the theoretical shift of the edge is approximately 1 eV greater than the experimental value. Previous authors^{11,15,16} have not included the effects of charge transfer explicitly.^{65,66} As in the present NA calculations, the shift in the optical edge was found to be greater than the experimental value.

Although our potentials have been adjusted to guarantee agreement with the experimental optical-absorption edge, the behavior of the 5-eV peak provides an independent test of the present calculations. In contrast with the edge, the interpretation of this peak has been controversial in Cu.^{61,62} Current views hold that the transitions associated with this peak arise from a large portion of the Brillouin zone and may be classified broadly as d -band \rightarrow conduction-band and conduction-band \rightarrow conduction-band transitions.⁶⁰ These include the transitions $X_5 \rightarrow X_4^l$, $L_1^l \rightarrow E_F$, and $L_{2'} \rightarrow L_1^u$, where the superscripts l and u refer, respectively, to the lower and upper L_1 levels.

Turning to Figs. 7(a) and 7(b), we examine the shifts for the charge-renormalized-atom and shifted-muffin-tin models with and without lattice dilatations. The effects of lattice dilatation are indicated by the vertical arrows in Fig. 7. They are seen to be sufficiently large that they must not be neglected in realistic calculations. Both models predict the $X_5 \rightarrow X_4^l$ and $L_1^l \rightarrow E_F$ transitions to move to lower energy faster than the $L_{2'} \rightarrow L_1^u$ transitions. As indicated in Fig. 7(b), the SMT model appears to agree with the experimental shifts rather well after lattice-dilatation effects have been included. However, its superiority with respect to the charge-renormalized-atom model in this connection may well be coincidental.

It seems plausible that the motion of the "Lower" peak to smaller energies in the experimental optical spectrum is due to changes in the d -band \rightarrow conduction-band transitions, as monitored in the present case by $L_1^l \rightarrow E_F$ and $X_5 \rightarrow X_4^l$. The "Upper" peak, on the other hand, may result from conduction-band \rightarrow conduction-band transitions (e.g., $L_{2'} \rightarrow L_1^u$). Contributions to this structure may also arise from d -band \rightarrow conduction-band transitions, particularly from the lower Σ_1 band to the Fermi level, which are found to be practically unaf-

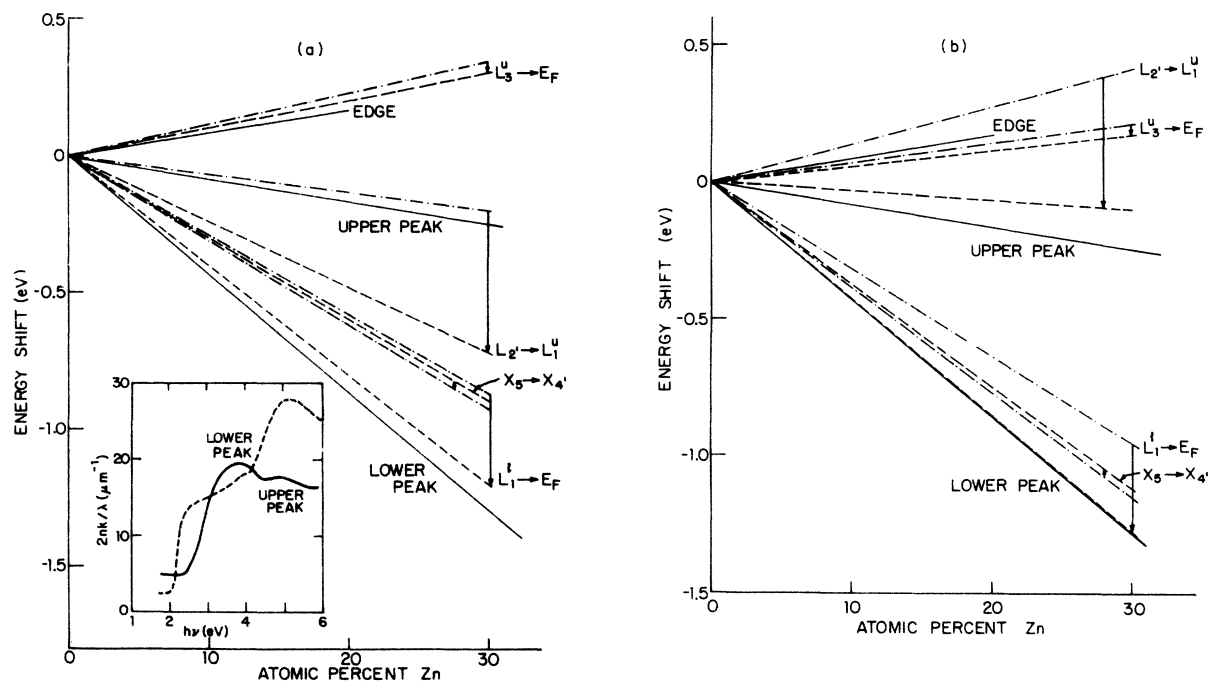


FIG. 7. Shifts with respect to Cu, in the dominant features of the experimental optical spectrum of α -CuZn, and the calculated changes in the energies of the principal optical transitions: (a) the CR model, and (b) the SMT model. The solid lines give the experimental results (Refs. 24 and 25). The dot-dashed lines refer to the calculated values without lattice expansion; the dashed lines give the calculated values corrected for lattice expansion. The inset shows the experimental optical-absorption curves of Ref. 25 for Cu (dashed line) and α -Cu_{0.68}Zn_{0.32} (solid line).

ected by alloying (cf. Fig. 4). This interpretation of changes in the large peak on alloying differs from that of Ref. 25 where it is suggested that the changes in the "Upper" peak result from the d -band-conduction-band transitions, while those in the "Lower" peak are due to the conduction-band-conduction-band transitions. Their considerations do not include the effects of charge transfer. Neither is the possibility that the d -band-conduction-band transitions may change on alloying considered.

While it may well be premature to speculate on such assignments in the absence of detailed calculations of the dielectric response function, the preceding interpretation suggests nevertheless that the study of optical structure as a function of concentration in various copper-based alloys may provide insight into the basic components contributing to the 5-eV and other peaks in this structure.

B. Fermi-surface properties

The Fermi-surface radii discussed in this section are obtained from a calculation of the Fermi energy that neglects the imaginary parts of the complex bands. Thus the effects of the broadening of the energy levels in the vicinity of the Fermi energy, as well as those of the broadening of the Cu d bands are neglected. Furthermore, as in

the case of a pure crystal, we assume each \vec{k} state in the common conduction band in the alloy to have a weight of unity. The validity of these approximations is further discussed in Appendix D. We emphasize, however, that a correct evaluation of the Fermi energy requires a calculation of the density of states, which as already mentioned is beyond the scope of the present paper.

Figure 8 presents the calculated values of $k_{1,0,0}$, $k_{1,1,0}$, and the neck radius, k_{Neck} , as a function of the Zn concentration in α -brass, for the charged-renormalized and the shifted-muffin-tin models, along with the results for the rigid-band model with the Cu density of states. Figure 8(a) shows the results without lattice expansion, while Fig. 8(b) includes lattice expansion, as calculated using the results of Ref. 47. The neck radii obtained from positron-annihilation experiments²⁶ for a range of Zn concentrations are also shown. The experimental points of Triftshauer *et al.* and Becker *et al.* (Ref. 26) are in fair agreement with our theoretical calculations and the rigid-band-model prediction. However, those of Williams *et al.* and Morinaga (Ref. 26) are rather lower than the other experiments as well as the theoretical predictions. A comparison of Figs. 8(a) and 8(b) shows that the expansion of lattice does have an effect on the Fermi-surface

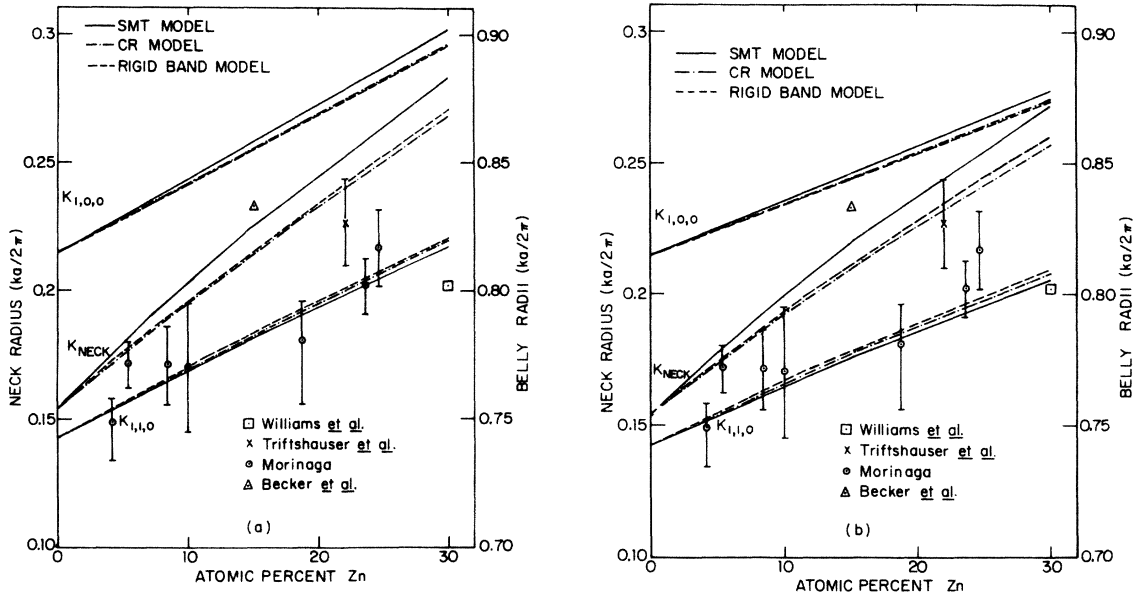


FIG. 8. Neck and belly radii in α - $\text{Cu}_x\text{Zn}_{1-x}$ as a function of the Zn concentration: (a) without lattice expansion, and (b) including the lattice-expansion effect using the results of Ref. 47. The solid lines and the dot-dashed lines refer to the SMT and the CS models, respectively, while the dashed lines give the results for the rigid-band model with the Cu density of states. The experimental data points (Ref. 26) for the neck radius are also shown.

properties of α -brass.

Figure 8 also shows that the various dimensions of the Fermi surface are insensitive to the choice of the model for charge transfer. The Fermi surface of Cu is seen to expand rather uniformly in all the directions in \vec{k} space. This feature is illustrated more clearly by Fig. 9, which shows the intersections of the Fermi surface of Cu and α - $\text{Cu}_{0.7}\text{Zn}_{0.3}$, with a few symmetry planes. The shading in Fig. 9 corresponds to six times the uncertainty in momentum on the Fermi surface of the alloy. The uncertainty in momentum, $\delta\vec{k}$, of a given state of momentum, \vec{k} , is related to its damping,³⁴ $\text{Im}\Sigma(\vec{k})$, by, $\delta\vec{k} = \text{Im}\Sigma(\vec{k})/\hbar v_F$, where the Fermi velocity v_F is estimated by assuming a free-electron band for the alloy.

The calculated values of the principal Fermi-

surface radii in α -brass are presented in Table III. The average dampings on the Fermi surface, the neck, and the [111] belly are also listed. As discussed in Sec. III B, the primary difference between the CR and the SMT models is once again seen to be in the magnitude of the damping. The results for the damping are compared with experiment in Sec. IV D below.

Chollet and Templeton²⁷ have measured the neck de Haas-van Alphen (dHvA) frequency, and the ratio of the [111] belly to the neck frequency in α -brass, for low concentrations of Zn. The experimental fractional increase in the neck radius of Cu [obtained by drawing a straight line through the CuZn data of Coleridge and Templeton (cf. Ref. 27)] is 3.0% per at.% Zn, which is to be compared with the calculated increase of $(2.6 \pm 0.4)\%$ and $(3.2$

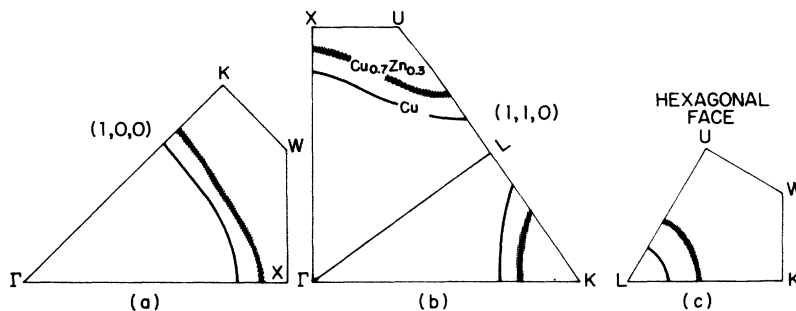


FIG. 9. Intersections of the Fermi surface of Cu (unshaded) and of α - $\text{Cu}_{0.7}\text{Zn}_{0.3}$ (shaded): (a) with a (1, 0, 0) plane, (b) with a (1, 1, 0) plane, and (c) with the hexagonal face of the Brillouin zone for the SMT model. The shading corresponds to six times the uncertainty in momentum on the Fermi surface of the alloy.

TABLE III. Fermi-surface properties for α -Cu_xZn_{1-x} having Cu lattice constant for different charge-transfer models. The Fermi-surface radii are given in units of $2\pi/a$, where a is the cube edge of the fcc Cu lattice. Average value of $\text{Im}\Sigma$ on the Fermi surface, [111] belly, and the neck is given in rydbergs.

	Cu _{0.85} Zn _{0.15}			Cu _{0.7} Zn _{0.3}	
	Cu	SMT	CR	SMT	CR
$k_{1,0,0}$	0.815	0.858	0.855	0.902	0.897
$k_{1,1,0}$	0.744	0.782	0.783	0.818	0.820
k_{Neck}	0.155	0.225	0.216	0.283	0.268
$\text{Im}\Sigma$ (FS)	0.0	-0.0032	-0.0091	-0.0068	-0.0147
$\text{Im}\Sigma$					
([111] belly)	0.0	-0.0034	-0.0090	-0.0074	-0.0150
$\text{Im}\Sigma$ (Neck)	0.0	-0.0028	-0.0087	-0.0065	-0.0141

$\pm 0.2\%$ per at. % Zn for the CR and the SMT models, respectively. Similarly, the experimental fractional decrease in the ratio of the [111] belly to neck radius [obtained by drawing a straight line through the CuZn data of Chollet and Templeton (cf. Ref. 27)] is 2.2% per at. % Zn, which compares reasonably with the calculated decrease of $(2.3 \pm 0.5)\%$ and $(2.8 \pm 0.25)\%$ per at. % Zn for the CR and the SMT models, respectively.

C. Other properties

In this subsection, we discuss the measurements of the Dingle temperature⁶⁷⁻⁶⁹ and the residual resistivity, which are related to the lifetimes of the electronic states in the alloy and hence to the imaginary parts of the complex band energies. The specific-heat measurements on α -brasses are also discussed briefly.

The Dingle temperature $x(\vec{k})$ is defined^{34, 56, 70}

$$x(\vec{k}) = \text{Im}\Sigma(\vec{k})/\pi k_B; \quad \text{Im}\Sigma(\vec{k}) = \hbar/2\tau_D; \quad (4.1)$$

where \vec{k} is the momentum of the state under consideration, k_B is the Boltzmann constant, and τ_D is the lifetime corresponding to the damping $\text{Im}\Sigma(\vec{k})$. The de Haas-Van Alphen experiments, which are possible only for very dilute alloys, measure an average of $x(\vec{k})$ over an extremal orbit on the Fermi surface, rather than $x(\vec{k})$ for a specific \vec{k} . However, a complete map of $x(\vec{k})$ on the Fermi surface can be obtained by inverting the de Haas-van Alphen data on a series of extremal orbits.^{58, 59} Unfortunately, such detailed experiments have not, as yet, been done on α -brass.

The theoretical map of $x(\vec{k})$ on the Fermi surface of the alloy is obtained from the complex band structure, by using Eq. (4.1). The Dingle temperature corresponding to a given orbit, which is to be compared with experiment, is then obtained by averaging $x(\vec{k})$ over the orbit in question. In α -brass with a maximum Zn concentration of 0.1 at. %, Coleridge and Templeton²⁷ experimentally obtain values of 20 and 15 °K/at. % Zn for the

Dingle temperatures x_N and x_B of the neck and the [111] belly orbits, respectively. The corresponding results of our calculations may be summarized as follows: for the SMT model, $x_N = 8.4$ °K/at. % Zn, $x_B = 11.1$ °K/at. % Zn, and $x_N/x_B = 0.76$; for the CR model, $x_N = 29.2$ °K/at. % Zn, $x_B = 30.2$ °K/at. % Zn and $x_N/x_B = 0.96$. The theory and experiment are seen to agree to within a factor of 2. In view of the sensitivity of the Dingle temperature to defects such as dislocations,⁷¹ it is difficult to interpret the experimental value of Dingle temperature as an intrinsic effect due to alloying alone. In addition, as already pointed out, the reliability of $\text{Im}\Sigma$ obtained from the present calculations is open to question because of its sensitivity to the atomic potentials of the constituents.

In contrast to the Dingle temperature, the residual resistivity is not related directly to the one-electron lifetime of the electronic states in the alloy. An actual evaluation of the conductivity lifetime τ_ρ for the nondilute alloy will not be attempted here. However, an estimate of the residual resistivity in the *low-Zn-concentration* limit is easy to make if the Fermi surface is assumed spherical and the necks are neglected. It is useful in providing insight into the validity of the phase shifts for Cu and Zn used in this paper for various models of charge transfer. Assuming the conduction electrons in the host to be free-electron-like, the residual resistivity may be obtained from the usual formula⁷²:

$$\rho = (2.732/k_F n_{\text{eff}}) \sum_{l=0}^{\infty} (l+1) \sin^2(\delta_l - \delta_{l+1}), \quad (4.2)$$

where ρ is given in the units $\mu\Omega \text{cm/at. \% impurity}$, k_F is the Fermi momentum in atomic units, and n_{eff} is the number of conduction electrons per atom in the host. Several authors⁵⁰ have estimated the residual resistivity for alloys using Eq. (4.2), with the phase shifts δ_l obtained by associating a square-well potential with the impurity, where the depth of the square well is chosen to satisfy the Friedel sum rule.⁷² One may alternatively associate the difference of the equivalent Cu- and Zn-muffin-tin potentials with the impurity, and calculate the phase shifts δ_l from it. Such a calculation for the present case yields for the SMT and the CR models a residual resistivity of 0.33 and 0.99 $\mu\Omega \text{cm/at. \% Zn}$. Morgan⁵⁵ and Coleridge⁵⁶ have shown that in the low-concentration limit, the difference of the impurity and the host phase shifts, $\delta_l = (\eta_l^i - \eta_l^h)$, should be associated with the scattering properties of the impurity. However, the effect of deviations from a spherical Fermi surface, which are neglected here, also play an important role in their results. Using $\delta_l \equiv \eta_l^{\text{Zn}} - \eta_l^{\text{Cu}}$ in Eq. (4.2) gives, for the SMT and the CR models, respectively, residual resistivities of 0.23 and 0.46

$\mu\Omega$ cm/at. % Zn. These estimates are to be compared with the experimental value³⁰ of 0.335 $\mu\Omega$ cm. As expected, the CR model yields a higher value in both cases.

The ratio $\beta \equiv \tau_\rho/\tau_D$ is expected to be greater than unity.^{73,74} Here τ_ρ is the resistivity lifetime, defined to be $\tau_\rho = m^*/ne^2\rho$, and τ_D is the Dingle-temperature lifetime given by Eq. (4.1). For simplicity, we take $m^* = 1.45 m$, the optical mass of Cu. The experimental value of the ratio β , obtained from experimental measurements of residual resistivity³⁰ and the Dingle temperature is 2.32–3.06, where the bounds on β correspond to using the experimental belly and neck Dingle temperatures for calculating the lifetime τ_D . The theoretical value of β (independent of the value of the effective mass m^*) is model dependent and varies between 1.6 and 4.2, which is in reasonable agreement with experiment. It should be emphasized again that the estimates of the residual resistivity above are qualitative rather than quantitative, because of the approximations involved in the use of Eq. (4.2) for calculating ρ .

The coefficient of the electronic specific heat γ , which is directly proportional to the density of states $\rho(E_F)$, at the Fermi level E_F is: $\gamma = \frac{1}{3}\pi^2 k_B^2 \rho(E_F)$, where k_B is Boltzmann's constant. Our calculated value of $\gamma = 0.61$ mJ mole⁻¹ °K⁻² for Cu is comparable with the experimental value²⁹ of (0.690 ± 0.002) mJ mole⁻¹ °K⁻². The discrepancy has been attributed to the electron-phonon interactions.²⁹ The low-temperature specific heat of α -brasses has been measured by Veal and Rayne,²⁸ and more recently by Mizutani *et al.*²⁹ These experiments show that the specific heat of Cu increases only by a small amount on alloying it with Zn, the maximum increase being about 3.5% of the specific heat of Cu. A calculation of γ requires knowledge of $\rho(E_F)$ which has not been evaluated explicitly in the present paper for the alloy. We can therefore only comment on other theoretical efforts.

We note that the rigid-band model with the Cu density of states cannot explain the experimental results on specific heat of α -brasses,⁴⁶ because

this model predicts a linear decrease with increasing Zn concentration, amounting to 10% of the specific heat of Cu for α -Cu_{0.7}Zn_{0.3}. Stern¹⁸ has attempted to explain the experimentally observed increase in γ for the Cu- and Ag-based alloys in terms of the enhancement of the density of states at the Fermi level, resulting from the presence of screening electrons around impurity atoms. Haga⁷⁵ has estimated the effect of the d -band broadening on the specific-heat coefficient of α -brass, using average Cu d -band damping $\text{Im}\Sigma(d \text{ band})$ as an adjustable parameter. To fit his theory to experimental results, he requires a value of $\text{Im}\Sigma(d \text{ band}) = 0.015$ Ry for the 30-at. % Zn alloy. This is comparable with the corresponding calculated value of 0.013 and 0.008 Ry for the typical d -band damping for the SMT and the CR models, respectively, and suggests that the broadening of energy levels has an important effect on the specific heat of α -brasses.

ACKNOWLEDGMENTS

We are grateful to C. D. Gelatt, S. Berko, D. Turnbull, A. R. Williams, and R. J. Higgins for helpful discussions concerning theoretical and/or experimental aspects of the problem. G. E. Juras and A. R. Williams were most obliging in communicating results prior to publication.

APPENDIX A

In this appendix we examine two formal aspects of the average t -matrix-KKR equations. We begin by establishing the relationship between Eq. (2.12) of the present paper and the (tight-binding) model Hamiltonian version of the ATA considered in Ref. 13. The generalization of Eq. (2.12) to the case of a virtual-crystal reference Hamiltonian is then discussed.

Equation (2.12) is the angular-momentum representation of the average- t -matrix secular equation. As Ziman⁷ has shown, this equation can be transformed into the more familiar reciprocal-lattice representation

$$|(|\vec{k} - \vec{K}_n|^2 - E)\delta_{nn'} + \Sigma_{nn'}(\vec{k}, E)| = 0, \quad (\text{A1a})$$

where

$$\Sigma_{nn'}(\vec{k}, E) = 4\pi(N/\Omega) \sum_l (2l+1) j_l(|\vec{k} - \vec{K}_n| R) \sigma_l(E) j_l(|\vec{k} - \vec{K}_{n'}| R) P_l(\cos\theta_{nn'}) \quad (\text{A1b})$$

and

$$\sigma_l(E) = \langle t_l(E) \rangle [1 + G_l^{(0)}(R, R) \langle t_l(E) \rangle]^{-1}. \quad (\text{A1c})$$

Here R is a constant usually taken to be the muffin-tin radius R_m , \vec{K}_n and $\vec{K}_{n'}$ are reciprocal-lattice vectors,

$$\langle t_l(E) \rangle \equiv \langle t_l(\kappa, \kappa) \rangle / j_l^2(\kappa R),$$

and $G_i^{(0)}(R, R)$ is a spherical matrix element of the free-particle Green's function

$$G_i^{(0)}(R, R) = \int Y_L(\vec{r}) [\delta(r-R)/R^2] G_0(|\vec{r}-\vec{r}'|) [\delta(r'-R)/R^2] Y_L(\vec{r}') d^3r d^3r' \\ = -\kappa j_i^2(\kappa R) [i - n_i(\kappa R)/j_i(\kappa R)], \quad (\text{A2})$$

and j_i and n_i are the spherical Bessel and Neumann functions, respectively.

Equations (A1) may be thought of as secular equations for a periodic lattice of effective potentials. Following Ziman⁷ and Soven,¹¹ these effective potentials can be interpreted in terms of non-local δ -function shell-model potentials:

$$v^{A(B)}(\vec{r}, \vec{r}') = \sum_L [\delta(r-R)/R^2] \\ \times Y_L(\vec{r}) v_i^{A(B)}(E) Y_L(\vec{r}') [\delta(r'-R)/R^2], \quad (\text{A3})$$

where the energy-dependent parameters $v_i^{A(B)}$ are chosen to guarantee that the model potential (A3) reproduces the proper scattering phase shifts¹¹

$$v_i^{A(B)}(E) = t_i^{A(B)}(E) [1 + G_i^{(0)}(R, R) t_i^{A(B)}(E)]^{-1}. \quad (\text{A4})$$

In view of this relation between $v_i(E)$ and $t_i(E)$, it is clear that the quantity $\Sigma_{nn'}(\vec{k}, E)$ in Eq. (A1b) is simply the matrix element (between plane-wave states $|\vec{k} + \vec{K}_n\rangle$ and $|\vec{k} + \vec{K}_{n'}\rangle$) of a periodic array of potentials of the form (A3), where the effective parameter v_i^{eff} is chosen to reproduce the average scattering matrix at each site, i. e.,

$$v_i^{\text{eff}}(E) = \langle t_i(E) \rangle [1 + G_i^{(0)}(R, R) \langle t_i(E) \rangle]^{-1} \equiv \sigma_i(E). \quad (\text{A5})$$

This result is the present version of the more general average- t -matrix expression for the self-energy operator,

$$\Sigma(E) = \sum_n \sigma_n(E), \quad (\text{A6})$$

$$\sigma_n = \langle t_n \rangle (1 + G_0 \langle t_n \rangle)^{-1},$$

employed in Ref. 13; and shows, once again, that the present calculations are based on an average- t -matrix approximation relative to an empty-lattice reference Hamiltonian.

As indicated in Sec. IIA, a more reliable average- t -matrix calculation is obtained if we begin with a virtual-crystal reference Hamiltonian. The alloy Hamiltonian is then written

$$\bar{G}_{LL'}(R, R) \equiv \int \int Y_L(\vec{r}) [\delta(r-R)/R^2] \bar{G}(\vec{r}, \vec{r}') [\delta(r'-R)/R^2] Y_{L'}(\vec{r}') d^3r d^3r'. \quad (\text{A12})$$

$\bar{G}_{LL'}(R, R)$ can be computed conveniently by using the formulas given by Soven⁸ [cf. Eqs. (48) and (49) of Soven's paper].

Using Eqs. (A9)–(A11), the summations in Eq. (A8) can be carried out simply. This leads to the secular equation,

$$|\delta_{LL'} - \langle \bar{t}_i(\kappa, \kappa) \rangle \bar{B}_{LL'}(\vec{k}, \kappa)| = 0, \quad (\text{A13})$$

$$H = \bar{H} + \sum_n [v_n^{A(B)}(\vec{r}) - \bar{v}_n(\vec{r})], \quad (\text{A7a})$$

where

$$\bar{H} = p^2/2m + \sum_n \bar{v}_n(\vec{r}) \quad (\text{A7b})$$

and

$$\bar{v}(\vec{r}) \equiv xv^A(\vec{r}) + (1-x)v^B(\vec{r}). \quad (\text{A7c})$$

$\bar{v}(\vec{r})$ is the atomic potential corresponding to the VC Hamiltonian (all quantities referring to the virtual crystal will be denoted by a bar). Beginning with Eqs. (A7), the scattering operator $\bar{T}(E)$ [cf. Eqs. (2.6) and (2.7)] may be rewritten

$$\bar{T} = \sum_n \langle \bar{t}_n \rangle + \sum_{\substack{n \\ m \neq n}} \langle \bar{t}_n \rangle \bar{G} \langle \bar{t}_m \rangle \\ + \sum_{\substack{n \\ m \neq n \\ p \neq m}} \langle \bar{t}_n \rangle \bar{G} \langle \bar{t}_m \rangle \bar{G} \langle \bar{t}_p \rangle + \dots \quad (\text{A8})$$

and

$$\langle \bar{t} \rangle = x\bar{t}^A + (1-x)\bar{t}^B, \quad (\text{A9})$$

where $\bar{t}^{A(B)}$ are the scattering matrices for $A(B)$ atoms with respect to the VC Hamiltonian, and are given by

$$\bar{t}^{A(B)} = \bar{v}^{A(B)} (1 - \bar{G} \bar{v}^{A(B)})^{-1}, \quad (\text{A10a})$$

where

$$\bar{v}^{A(B)}(\vec{r}) \equiv [v^{A(B)}(\vec{r}) - \bar{v}(\vec{r})]. \quad (\text{A10b})$$

Equations (A8)–(A10) can be solved easily provided we use δ -function shell-model pseudopotentials of the form given by Eqs. (A3) and (A4). For example, Eq. (A10) gives

$$\bar{t}_i^{A(B)}(E) = \bar{v}_i^{A(B)}(E) [1 - \bar{G}_{LL'}(R, R) \bar{v}_i^{A(B)}(E)]^{-1}, \quad (\text{A11})$$

where $\bar{v}_i^{A(B)}(E)$ are chosen to reproduce the scattering phase shifts of the difference potential $v^{A(B)} - \bar{v}$, and $\bar{G}_{LL'}(R, R)$ is the angular-momentum component of the VC Green's function,

where

$$\bar{B}_{LL'}(\vec{k}, \kappa) = [j_l(\kappa R) j_{l'}(\kappa R)]^{-1} \sum_{\vec{R}_n \neq 0} \int e^{i\vec{k} \cdot \vec{R}_n} \bar{G}(\vec{r} + \vec{R}_n, \vec{r}') Y_L(\vec{r}) Y_{L'}(\vec{r}') d\Omega_r d\Omega_{r'} \quad (\text{A14})$$

and $r = r' = R$.

Equations (A13) and (A14) give the AKKR equation with respect to the VC reference Hamiltonian. It should be emphasized that the assumption of a δ -function shell-model potential is necessary in order that the series (A8) can be summed explicitly. By contrast, this assumption is not necessary to sum the series (2.6) which involves G_0 instead of \bar{G} .

APPENDIX B

This appendix presents the details of the Cu and Zn potentials used in this paper.

The lattice constant for Cu is taken to be 6.8309 a. u.⁴⁷ The renormalized-atom potentials (see Sec. IIB for an outline of the method) of Cu and Zn were generated on the Herman-Skillman mesh.⁷⁶ This method yields the spherically symmetric crystalline potential, defined within the Wigner-Seitz sphere. The l -dependent muffin-tin zero is calculated by averaging the potential between the muffin tin and the Wigner-Seitz sphere radii. The s and the d muffin tins, V_0^s and V_0^d , for Cu are -0.8341 and -0.9456 Ry. The corresponding values of V_0^s and V_0^d for Zn are -0.8128 and -1.0449 Ry, respectively.

The muffin-tin zero for the alloy is taken to be the average of the s -muffin-tin zeros of the constituents, i. e.,

$$\bar{V}_0 = xV_0^s(\text{Cu}) + (1-x)V_0^s(\text{Zn}).$$

As discussed in Sec. IIA, this corresponds to the use of the VCA outside the muffin-tin spheres. The use of the s , rather than the d muffin tin, is natural because the s - p -like electrons, due to the extended nature of their wave functions, sample the muffin-tin region much more than the tight-binding d -like electrons.

APPENDIX C

In this appendix, we show that the charged-renormalized (CR) model gives numerical results for α -Cu _{x} Zn _{$1-x$} , which are very close to the results for a model in which the transferred charge is assumed to be confined to a shell placed at the muffin-tin radius. This model has been briefly discussed in Sec. IIB. Since this charged-shell (CS) model involves a constant shift of the potential inside the muffin-tin sphere, it is much simpler to implement than the CR model, which requires an actual calculation of a new potential corresponding to the charged atoms.

Table IV shows that for α -Cu_{0.7}Zn_{0.3}, the complex energy levels for the CS and the CR models agree with each other to within a few hundredths of an electron volt. In view of this, most of the calculations in this paper for the CR model were actually done by using the simpler CS model. The agreement between the two models can be clarified by considering the shift in potential $\delta V(r) \equiv v_c(r) - v_n(r)$ (cf. Fig. 10) associated with constructing charged-renormalized atoms. The subscripts c and n refer to the charged-renormalized and the neutral-atom potential, respectively. The top curves in Fig. 10 are for Cu, with $\Delta^{\text{Cu}} = +0.08$, while the lower curve is for Zn, with $\Delta^{\text{Zn}} = -0.226$. Only 4s charge transfer is considered. The shifts $\delta V(r) = e^2 \Delta^{\text{Cu (Zn)}} / R_m$ corresponding to the CS model are also shown. Figure 10 shows that the shifts in potential associated with CR model are rather smoothly varying as a function of r , particularly in the "d region" around 1 a. u., which is of primary concern to the d -band properties. This implies that the net effect of the adjustments in the CR model is to merely shift the d bands of Cu upwards and those of Zn downwards, in a manner similar to the CS model. However, it should be emphasized that even though the final energy bands for the two models are quantitatively similar, the magnitude of charge $\Delta^{\text{Cu (Zn)}}$, required to obtain agreement with the experimental optical edge is different for the two models. The CS and the CR models require Δ^{Cu} of 0.072 and 0.057, respectively, for α -Cu_{0.7}Zn_{0.3}. This difference may also be understood by a reference to Fig. 10, which

TABLE IV. Comparison of the complex energy levels for the CR and CS models for α -Cu_{0.7}Zn_{0.3}. Complex energies are denoted as in Table I.

State	Charged renormalized (CR)	Charged shell (CS)
Γ_1	(-0.0275, 0.0)	(-0.0297, 0.0)
$\Gamma_{25'}$	(0.4397, -0.0058)	(0.4398, -0.0061)
Γ_{12}	(0.4892, -0.0076)	(0.4894, -0.0075)
X_1	(0.3123, -0.0042)	(0.3141, -0.0044)
X_3	(0.3520, -0.0041)	(0.3535, -0.0041)
X_2	(0.5240, -0.0085)	(0.5238, -0.0085)
X_5	(0.5360, -0.0088)	(0.5357, -0.0086)
$X_{4'}$	(0.7904, -0.0143)	(0.7894, -0.0163)
L_1^I	(0.3134, -0.0068)	(0.3150, -0.0074)
L_3^I	(0.4355, -0.0060)	(0.4359, -0.0060)
L_5^I	(0.5262, -0.0085)	(0.5259, -0.0084)
$L_{2'}$	(0.5771, -0.0098)	(0.5758, -0.0112)

shows that for a given magnitude of $\Delta^{\text{Cu (Zn)}}$, the shift of the potential in the "d region" for the CR model is larger than that for the CS model. Hence, in order to bring about a given shift in the position of the Cu d band (determined so as to give agreement with the experimental optical edge) a smaller value of $\Delta^{\text{Cu (Zn)}}$ is required in the CR model.

Finally, we remark that the changes in the potential for the CR model (i. e., δV_s^{Cu} , δV_s^{Zn} , and δV_d^{Zn}) are given very well by the electrostatic potential in a uniformly charged Wigner-Seitz sphere, with total charge $\Delta^{\text{Cu (Zn)}}$. This is expected, since the 4s charge is rather uniformly spread out within the Wigner-Seitz sphere. δV_d^{Cu} differs from δV_s^{Cu} (or from the electrostatic potential in a uniformly charged Wigner-Seitz sphere with a total charge Δ^{Cu}) by a maximum of only 8%, at the Wigner-Seitz radius, and much less in the "d region" around 1 a. u.

APPENDIX D

In this appendix the methods used for calculating the complex energy bands and the Fermi energy for α -brass are discussed.⁷⁷

The real crystal bands are considered first. The KKR determinant, $F(E, \vec{k})$, may be written

$$F(E, \vec{k}) = \left| A_{LL'}(\vec{k}, E) + (E)^{1/2} \cot \eta_l(E) \delta_{LL'} \right|, \quad (\text{D1})$$

where $A_{LL'}$ are the real structure functions,³³ and η_l is the l th phase shift. Equation (D1) explicitly shows that $F(E, \vec{k})$ is real for $E > 0$. It also shows that $F(E, \vec{k})$ is real for $E < 0$, because for $E < 0$, $(E)^{1/2}$ and $\cot \eta_l(E)$ are both pure imaginary, and hence $(E)^{1/2} \cot \eta_l(E)$ is real. We calculate the structure functions $A_{LL'}$ using the method described by Ham and Segall.³³ The roots of $F(E, \vec{k})$, for a given \vec{k} , are located by fitting $F(E, \vec{k})$ to a monomial of the form $(\text{const})(E - E_0)^n$, in the neighborhood of an n -fold-degenerate root at energy E_0 . The roots are calculated to an accuracy of approximately 10^{-4} Ry.

The \vec{k} -space integration method⁷⁸ is used to calculate the Fermi level in Cu. This method is especially suited for Cu, because the Fermi surface of Cu consists of a single sheet. In this method, a number of directions (45 in the present calculation) are chosen in the basic wedge in \vec{k} space, which comprises $\frac{1}{48}$ th of the Brillouin zone of an fcc lattice. In each of these directions, the energy eigenvalues for four different k values are calculated. The k values are chosen in such a way that the corresponding energy eigenvalues enclose a range of energies around the Fermi energy. These are the only roots (180 in the present calculation) calculated for obtaining the Fermi surface and its properties. For a given energy, the radius $\vec{k}(E)$ of the constant-energy surface in the direction \vec{k} , is obtained by interpolation, using the four k values, and corresponding energy eigenvalues that were calculated for this particular

direction in \vec{k} space. In order to improve the accuracy of the \vec{k} -space integration method, we carry out further interpolations to obtain 516 points on the constant-energy surface from the starting 45 points. An accuracy of 10^{-3} Ry is expected in the evaluation of the Fermi energy. The same set of roots is also used to calculate the density of states in a small range of energies around E_F .

The preceding discussion for Cu will now be used to consider the AKKR equation [cf. Eq. (2.12)] which is obtained from Eq. (D1) by replacing η_l by $\bar{\eta}_l$, where $\bar{\eta}_l$ is the phase shift corresponding to the average t matrix $\langle t \rangle$,

$$\begin{aligned} \langle t \rangle &= xt^A + (1-x)t^B \\ &= -\kappa^{-1}x(\cot \eta^A - i)^{-1} - \kappa^{-1}(1-x)(\cot \eta^B - i)^{-1} \\ &\equiv -\kappa^{-1}(\cot \bar{\eta} - i)^{-1}, \end{aligned} \quad (\text{D2})$$

where $\kappa = (E)^{1/2}$. Equation (D2) can be rewritten in the form

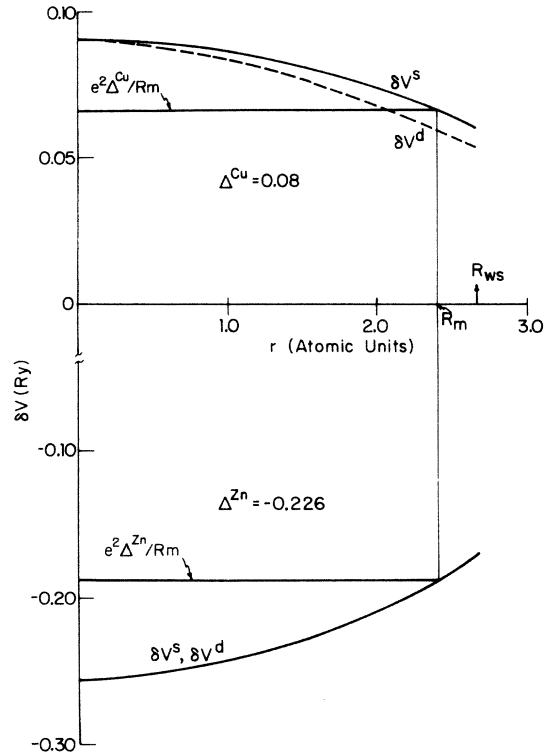


FIG. 10. Shift in potential, $\delta V(r) \equiv v_c(r) - v_n(r)$, where the subscripts c and n refer to the charged-renormalized and the neutral-atom potentials, respectively. The top curves give δV_s (solid) and δV_d (dashed) for Cu, with $\Delta^{\text{Cu}} = 0.08$; the bottom curve gives δV_s and δV_d for Zn with $\Delta^{\text{Zn}} = -0.226$. The square wells correspond to $e^2 \Delta^{\text{Cu (Zn)}} / R_m$, which represents a constant shift in potential corresponding to a shell of total charge $\Delta^{\text{Cu (Zn)}}$ placed at R_m [referred to as charged shell (CS) model in the text]. Only 4s charge transfer is considered.

$$\cot\bar{\eta} = i + [x(\cot\eta^A - i)^{-1} + (1-x)(\cot\eta^B - i)^{-1}]^{-1}, \quad (\text{D3})$$

where $\cot\bar{\eta}$ and therefore the determinant $\bar{F}(E, \vec{k})$ of the AKKR equation are in general complex functions of the energy. We solve the AKKR equation for complex E , as a function of real \vec{k} . Although it is conceptually equivalent to consider complex \vec{k} as a function of real E ,³⁶ it is not clear how one can do this within the framework of the AKKR equation, because the structure functions A_{LL} are not defined for complex \vec{k} . By contrast, A_{LL} are well defined³³ for complex E . To evaluate $\bar{F}(E, \vec{k})$, one needs the phase shifts of the constituents at complex energies in addition to the structure functions. The phase shifts are well defined for complex energies; the t matrix is, in fact, an analytic function of the complex energy E , except for poles corresponding to the bound-state energies. In the present calculation, the value of t matrix for a complex E is obtained by making a Taylor series expansion around the real part of E . The derivatives of the function needed in the Taylor series expansion are calculated by using the values of the t matrix along the real energy axis. The roots of the function $\bar{F}(E, \vec{k})$ are calculated by using methods very similar to those discussed above for the real case. In particular, the complex roots are located, once again by fitting $\bar{F}(E, \vec{k})$ to a monomial of the form $(\text{const})(E - E_0)^n$, where E_0 is now a complex

number.

For calculating the Fermi energy of the alloy, the imaginary part of the complex energy bands is neglected. Once this approximation is made the calculation of the Fermi surface of α -brass proceeds in a manner identical to the corresponding calculation for Cu. The Fermi level E_F for the alloy is determined by requiring that the volume enclosed by the constant-energy surface $\vec{k}(E_F)$ be such that it can accommodate $(2-x)$ electrons/atom, where x is the concentration of Cu atoms. As already noted, a correct evaluation of E_F requires a calculation of the density of states, $\rho(E)$. However, for the CuZn system the maximum broadening of the energy levels at the Fermi energy is comparable to the thermal broadening at room temperature, and may to a good approximation be neglected in calculating E_F . Furthermore, the separation between the Fermi energy and the center of gravity of the Cu d bands ($E_F - E_d^{\text{Cu}}$) is much larger than the average damping of the Cu d bands, $\text{Im}\Sigma_d^{\text{Cu}}$. In fact, even for $\text{Cu}_{0.7}\text{Zn}_{0.3}$

$$(E_F - E_d^{\text{Cu}})/\text{Im}\Sigma_d^{\text{Cu}} \approx 30.$$

Consequently, even though the Cu d states broaden on alloying, most of the weight of their spectral density is contained below E_F . Hence, our evaluation of E_F is not expected to be affected seriously by the broadening of the d bands.

*Work supported in part by Grant No. GH-32774 of the National Science Foundation.

†Work supported in part by Grant No. GH-35691 of the National Science Foundation.

‡Work supported by the U. S. Atomic Energy Commission.

¹P. Soven, Phys. Rev. **156**, 809 (1967); D. W. Taylor, Phys. Rev. **156**, 1017 (1967); Y. Onodera and Y. Toyozawa, J. Phys. Soc. Jap. **24**, 341 (1968); B. Velický, S. Kirkpatrick, and H. Ehrenreich, Phys. Rev. **175**, 747 (1968); F. Yonezawa, Progr. Theor. Phys. **40**, 734 (1968); P. Soven, Phys. Rev. **178**, 1136 (1969).

²J. Friedel, Can. J. Phys. **34**, 1190 (1956); P. W. Anderson, Phys. Rev. **124**, 41 (1961).

³J. Hubbard, Proc. Roy. Soc. A **276**, 238 (1963); Proc. Roy. Soc. A **277**, 237 (1964); Proc. Roy. Soc. A **281**, 401 (1964).

⁴S. Kirkpatrick, B. Velický, and H. Ehrenreich, Phys. Rev. B **1**, 3250 (1970); G. M. Stocks, R. W. Williams, and J. S. Faulkner, Phys. Rev. Lett. **26**, 253 (1971); Phys. Rev. B **4**, 4390 (1971); M. P. Das and S. K. Joshi, Phys. Rev. B **4**, 4363 (1971); G. M. Stocks, R. W. Williams, and J. S. Faulkner, J. Phys. F **3**, 1688 (1973).

⁵D. Stroud and H. Ehrenreich, Phys. Rev. B **2**, 3197 (1970).

⁶K. Levin and H. Ehrenreich, Phys. Rev. B **3**, 4172 (1971); F. Brouers and A. V. Vedyayev, Phys. Rev. B **5**, 348 (1972); C. D. Gelatt and H. Ehrenreich, Bull. Am. Phys. Soc. **18**, 94 (1973).

⁷M. Lax, Rev. Mod. Phys. **23**, 287 (1951); P. C. Waterman and R. Truell, J. Math. Phys. **2**, 512 (1961); S. F. Edwards, Proc. Roy. Soc. A **267**, 518 (1962); J. M.

Ziman, Proc. Phys. Soc. Lond. **86**, 337 (1965); B. L. Gyorffy, Phys. Rev. B **1**, 3290 (1970); L. Schwartz and H. Ehrenreich, Ann. Phys. **64**, 100 (1971); D. E. Thornton, Phys. Rev. B **4**, 3371 (1971).

⁸P. Soven, Phys. Rev. B **2**, 4715 (1970); H. Shiba, Progr. Theor. Phys. **46**, 77 (1971); B. L. Gyorffy, Phys. Rev. B **5**, 2382 (1972).

⁹J. Korringa, J. Phys. Chem. Solids **7**, 252 (1958).

¹⁰J. L. Beeby, Phys. Rev. **135**, A130 (1964); Proc. Roy. Soc. A **279**, 82 (1964); Proc. Roy. Soc. A **302**, 113 (1967).

¹¹P. Soven, Phys. Rev. **151**, 539 (1966).

¹²M. M. Pant and S. K. Joshi, Phys. Rev. B **1**, 2532 (1970); Phys. Rev. B **2**, 1704 (1970).

¹³L. Schwartz, F. Brouers, A. V. Vedyayev, and H. Ehrenreich, Phys. Rev. B **4**, 3383 (1971).

¹⁴J. Korringa, Physica **13**, 392 (1947); W. Kohn and N. Rostoker, Phys. Rev. **94**, 1111 (1954).

¹⁵H. Amar, K. H. Johnson, and C. B. Sommers, Phys. Rev. **153**, 655 (1967); H. Amar, K. H. Johnson, and K. P. Wang, Phys. Rev. **148**, 672 (1966).

¹⁶M. M. Pant and S. K. Joshi, Phys. Rev. **184**, 635 (1969).

¹⁷L. Nordheim, Ann. Phys. **9**, 607 (1931); Ann. Phys. **9**, 641 (1931).

¹⁸E. A. Stern, Phys. Rev. **144**, 545 (1966); Phys. Rev. B **1**, 1518 (1970); Phys. Rev. Lett. **26**, 1630 (1971).

¹⁹A. R. Miedema, F. R. de Boer, and P. F. de Chatel, J. Phys. F **3**, 1558 (1973).

²⁰R. E. Watson, J. Hudis, and M. L. Perlman, Phys. Rev. B **4**, 4139 (1971).

- ²¹N. F. Mott, Proc. Phys. Soc. Lond. **49**, 258 (1937); F. J. Arlinghaus, Phys. Rev. **157**, 491 (1967); A. R. Williams (private communication).
- ²²W. B. Pearson, *A Handbook of Lattice Spacings and Structures of Metals and Alloys* (Pergamon, New York, 1958).
- ²³R. E. Watson, H. Ehrenreich, and L. Hodges, Phys. Rev. Lett. **24**, 829 (1970); L. Hodges, R. E. Watson, and H. Ehrenreich, Phys. Rev. B **5**, 3953 (1972).
- ²⁴M. A. Bionde and J. A. Rayne, Phys. Rev. **115**, 1522 (1959).
- ²⁵G. P. Pells and H. Montgomery, J. Phys. C **3**, S330 (1970).
- ²⁶D. L. Williams, E. H. Becker, and P. Petijevich, Bull. Am. Phys. Soc. **14**, 402 (1969); B. W. Murry and J. D. McGervey, Phys. Rev. Lett. **24**, 9 (1970); W. Triftshausner and A. T. Stewart, J. Phys. Chem. Solids **32**, 2717 (1971); H. Morinaga, J. Phys. Soc. Jap. **33**, 996 (1972); E. H. Becker, P. Petijevich, and D. L. Williams, J. Phys. F **1**, 806 (1971).
- ²⁷L. F. Chollet and I. M. Templeton, Phys. Rev. **170**, 656 (1968); I. M. Templeton, P. T. Coleridge, and L. F. Chollet, Phys. Kondens. Materie **9**, 21 (1969); P. T. Coleridge and I. M. Templeton, Can. J. Phys. **49**, 2449 (1971).
- ²⁸B. W. Veal and J. A. Rayne, Phys. Rev. **130**, 2156 (1963).
- ²⁹U. Mizutani, S. Noguchi, and T. B. Massalski, Phys. Rev. B **5**, 2057 (1972).
- ³⁰J. O. Linde, Ann. Phys. **15**, 219 (1932).
- ³¹W. R. G. Kemp, P. G. Klemens, R. J. Tainsh, and G. K. White, Acta Met. **5**, 303 (1957).
- ³²The assumption of randomness is only approximately valid in practice. Experimental evidence points to the existence of short-range order in α -brass; see, for example, E. Lang and W. Schüle, Z. Metallkde. **61**, 866 (1970).
- ³³F. S. Ham and B. Segall, Phys. Rev. **124**, 1786 (1961); B. Segall and F. S. Ham, *Methods in Computational Physics*, edited by B. Alder, S. Fernbach, and M. Rotenberg (Academic, New York, 1968), Vol. 8.
- ³⁴In terms of the spectral density functions $\rho(\vec{k}, E)$, this situation would correspond to a well-defined peak whose center and width are specified by $E_1(\vec{k})$ and $E_2(\vec{k})$, respectively. The imaginary part of the self-energy $\text{Im } \Sigma(\vec{k})$ is taken to be equal to $E_2(\vec{k})$.
- ³⁵Essentially the same secular determinant as Eq. (2.12) was proposed by Ziman (cf Ref. 36) for calculating the quasiparticle spectrum for a liquid, with the natural modification that the sum in Eq. (2.11) is replaced by an integral weighted by the pair distribution function of the liquid.
- ³⁶J. M. Ziman, Proc. Phys. Soc. Lond. **88**, 387 (1966).
- ³⁷C. Kittel, *Introduction to Solid State Physics* (Wiley, New York, 1968).
- ³⁸Previous VC calculations (cf. Refs. 15 and 16) have avoided this unphysical behavior only by artificially assuming the Cu d bands to remain unchanged. Such an approximation is not necessary in ATA.
- ³⁹The interpolation scheme of Hodges *et al.* (cf. Ref. 40) was also applied to the real parts of the complex bands, and the d -overlap parameters were found to decrease linearly on alloying.
- ⁴⁰L. Hodges, H. Ehrenreich, and N. D. Lang, Phys. Rev. **152**, 505 (1966); L. Hodges, Ph.D. thesis (Harvard University, 1966) (unpublished).
- ⁴¹A. H. Lettington, Philos. Mag. **11**, 863 (1965).
- ⁴²J. Friedel, Adv. Phys. **3**, 461 (1954); Ann. Phys. **9**, 158 (1954).
- ⁴³ E_{Γ_1} is found to follow the VCA result, i.e., $\Gamma_1^{\text{alloy}} \cong \Gamma_1^{\text{VC}} \cong x\Gamma_1^{\text{Cu}} + (1-x)\Gamma_1^{\text{Zn}}$, where Γ_1^{Zn} refers to the hypothetical crystal of Zn on a Cu lattice. Γ_1^{Cu} and Γ_1^{Zn} are calculated to be 0.0161 and -0.0557 Ry, giving $\Gamma_1^{\text{VC}} = -0.0055$ Ry for the 30 at. % Zn alloy, which compares well with the calculated value of -0.009 Ry for the NA model. The energy gaps at the zone faces (e.g., L_1-L_2') are also found to vary linearly between their values for pure Cu and Zn on the Cu lattice.
- ⁴⁴N. F. Mott and H. Jones, *The Properties of Metals and Alloys* (Dover, New York, 1958).
- ⁴⁵N. F. Mott, Adv. Phys. **13**, 325 (1964).
- ⁴⁶J. M. Ziman, Adv. Phys. **10**, 1 (1961).
- ⁴⁷H. L. Davis, J. S. Faulkner, and H. W. Joy, Phys. Rev. **167**, 601 (1968).
- ⁴⁸Davis *et al.* (cf. Ref. 47) constructed a somewhat artificial potential which is guaranteed to give the correct Fermi surface. The present potential was not constructed as judiciously. However, the same accuracy could have been achieved by choosing the renormalization factor to be weakly r dependent.
- ⁴⁹J. Friedel, Adv. Phys. **3**, 446 (1954); P. de Faget de Casteljau and J. Friedel, J. Phys. Rad. **17**, 27 (1956).
- ⁵⁰F. J. Blatt, Phys. Rev. **108**, 285 (1957); C. M. Hurd and E. M. Gordon, J. Phys. Chem. Solids **29**, 2205 (1968); J. H. Tripp and D. E. Farrell, Phys. Rev. **7**, 571 (1973).
- ⁵¹P. Roman, *Advanced Quantum Theory* (Addison-Wesley, Reading, Mass., 1965), Sec. 3.3.
- ⁵²J. M. Ziman, Phys. Rev. **121**, 1320 (1961).
- ⁵³S. Kirkpatrick, Phys. Rev. B **3**, 2563 (1971).
- ⁵⁴K. H. Johnson, Phys. Lett. A **27**, 138 (1968); R. Harris, J. Phys. C **3**, 172 (1970); J. Phys. F **3**, 89 (1973).
- ⁵⁵G. J. Morgan, Proc. Roy. Soc. Lond. **89**, 365 (1966).
- ⁵⁶P. T. Coleridge, J. Phys. F **2**, 1016 (1972); Phys. Rev. B **7**, 3508 (1973).
- ⁵⁷An excellent source of references is the review article by M. Springford [Adv. Phys. **20**, 493 (1971)].
- ⁵⁸D. H. Lowndes, K. Miller, and M. Springford, Phys. Rev. Lett. **25**, 1111 (1970).
- ⁵⁹B. Bosacchi, J. B. Ketterson, and L. R. Windmiller, Phys. Rev. B **5**, 3816 (1972).
- ⁶⁰F. M. Mueller and J. C. Phillips, Phys. Rev. **157**, 600 (1967); C. Y. Fong, M. L. Cohen, R. R. L. Zucca, J. Stokes, and Y. R. Shen, Phys. Rev. Lett. **25**, 1486 (1970); A. R. Williams, J. F. Janak, and V. L. Moruzzi (unpublished).
- ⁶¹U. Gerhardt, D. Beaglehole, and R. Sandrock, Phys. Rev. Lett. **19**, 309 (1967); U. Gerhardt, Phys. Rev. **172**, 651 (1968).
- ⁶²H. Ehrenreich and H. R. Philipp, Phys. Rev. **128**, 1622 (1962); D. Beaglehole, Proc. Phys. Soc. **87**, 461 (1966); G. P. Pells and M. Shiga, J. Phys. C **2**, 1835 (1969).
- ⁶³D. E. Eastman and J. K. Cashion, Phys. Rev. Lett. **24**, 310 (1970); I. Lindau and L. Waldén, Solid State Commun. **9**, 1147 (1971).
- ⁶⁴See, for example, J. W. D. Connolly, Phys. Rev. **159**, 415 (1967).
- ⁶⁵In Refs. 11 and 16, the crystalline Cu and Zn potentials are constructed by overlapping the atomic potentials (cf. Ref. 66). In general, the Wigner-Seitz cell in such a calculation will not be neutral, and the charge transfer

is implicitly included to some extent.

- ⁶⁶L. F. Mattheiss, Phys. Rev. 134, 192 (1964).
- ⁶⁷R. B. Dingle, Proc. Roy. Soc. A 211, 517 (1962).
- ⁶⁸P. E. King Smith, Philos. Mag. 12, 1123 (1965).
- ⁶⁹A good recent source of references is: *Proceedings of an International Conference on Electron Mean Free Paths in Metals, Zurich, Switzerland*, 1968 (Springer, Berlin, 1969); also Phys. Kondens. Mater. 9 (1969).
- ⁷⁰E. Mann, Phys. Kondens. Mater. 12, 210 (1971); P. Soven, Phys. Rev. B 5, 260 (1972).
- ⁷¹D. W. Terwillinger and R. J. Higgins, Phys. Rev. B 7, 667 (1973); R. A. Phillips, and A. V. Gold, Phys. Rev. 178, 932 (1969).
- ⁷²C. Kittel, *Quantum Theory of Solids*, (Wiley, New York, 1963), Chap. 18.
- ⁷³A. D. Brailsford, Phys. Rev. 149, 456 (1966).
- ⁷⁴J. S. Dugdale and Z. S. Basinski, Phys. Rev. 157, 552 (1967).
- ⁷⁵E. Haga, Proc. Phys. Soc. Lond. 91, 169 (1967); J. Phys. C 1, 795 (1968).
- ⁷⁶F. Herman and S. Skillman, *Atomic Structure Calculations* (Prentice-Hall, Englewood Cliffs, N. J., 1963).
- ⁷⁷All the calculations in this paper have been done using $l \leq 2$ phase shifts.
- ⁷⁸J. S. Faulkner, H. L. Davis, and H. W. Joy, Phys. Rev. 161, 656 (1967).

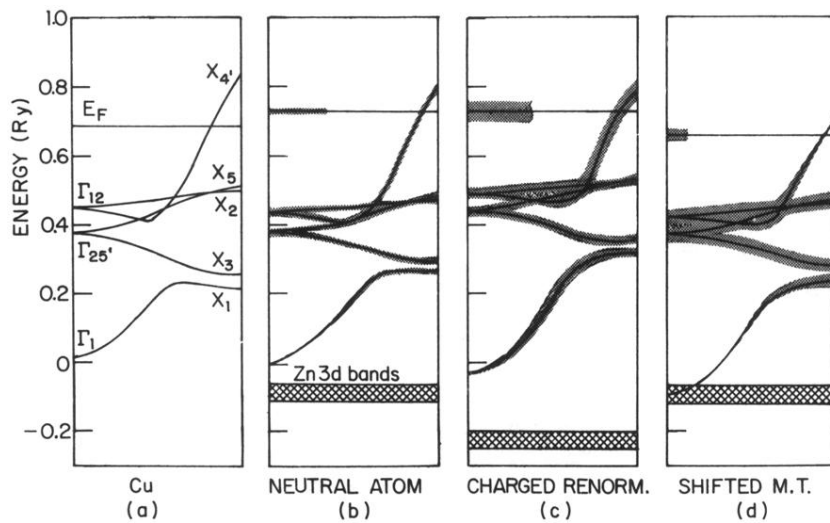


FIG. 3. Calculated energy bands for pure Cu and α -Cu_{0.7}Zn_{0.3} from $\Gamma \rightarrow X$: (a) pure Cu, (b)–(d) α -Cu_{0.7}Zn_{0.3} for different charge-transfer models. The shading of the bands corresponds to four times the imaginary part of the complex energies. The shading around the Fermi energy corresponds to four times the average damping on the Fermi surface. The Zn 3d bands are shown as a hatched band. The energy zero is taken to be -0.8341 Ry.

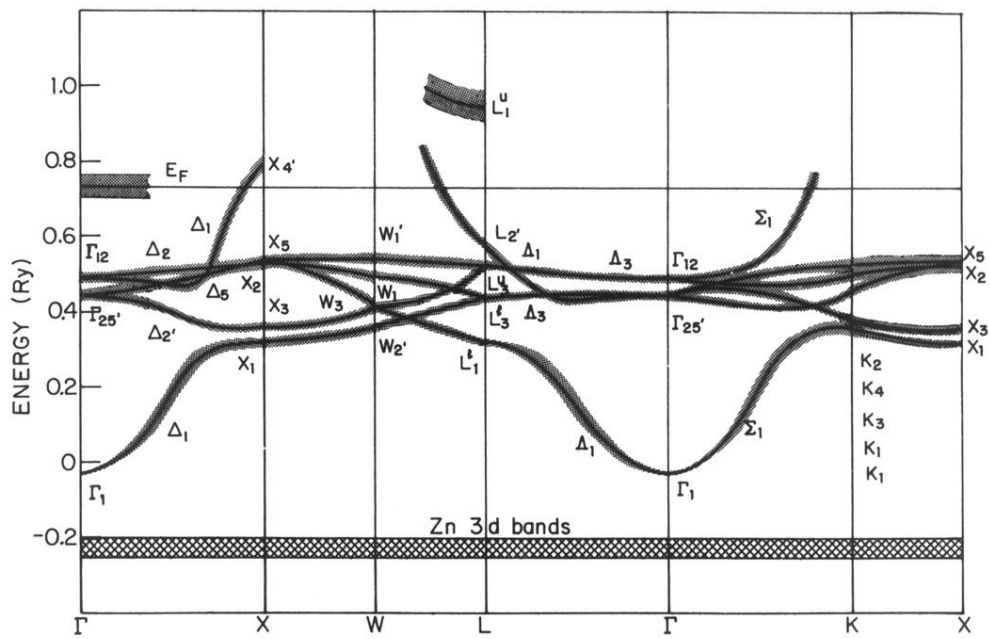


FIG. 4. Calculated energy bands for $\alpha\text{-Cu}_{0.7}\text{Zn}_{0.3}$ for the charged-renormalized atom model. See caption for Fig. 3 for the meaning of the shading.